Electronic Supplementary Material (ESI) for ChemComm.

Supporting information

Tungsten imido catalysts for selective ethylene dimerisation

Christopher M. R. Wright, Zoë R. Turner, Jean-Charles Buffet and Dermot O'Hare*

Table of Contents

1. Experimental Details

General details

All manipulations were performed in a MBraun Unilab glove box or using standard Schlenk techniques under an inert N_2 atmosphere. Reaction solvents (benzene, toluene, hexane) were dried using an MBraun SPS 800 solvent purification system and stored on either 3 Å molecular sieves (benzene) or potassium mirror (toluene, hexane) in pre-dried glass Rotaflo or Young's tap ampoules. Anhydrous pyridine (Sigma Aldrich) was stored on 3 Å molecular sieves in a pre-dried glass Rotaflo ampoule. Ethylene was dried over a column containing 3 Å molecular sieves. C_6D_6 (Sigma Aldrich) was dried over NaK, vacuum transferred and freeze-pump-thaw degassed prior to use. C_4D_8O was dried over calcium hydride, filtered and stored over 3 Å molecular sieves.

Solution phase NMR spectroscopy

NMR spectra were measured on a 400 MHz Bruker Avance III HD NanoBay spectrometer. ^1H and $^{13}C\{^1H\}$ NMR spectra were recorded at 25 °C and referenced internally to the residual protio-solvent resonance of the deuterated solvent used. ^1H and $^{13}C\{^1H\}$ chemical shifts, δ, are given in parts per million (ppm).

Elemental analysis

Elemental analysis (CHN) was performed by Mr. Stephen Boyer at London Metropolitan University, North Campus, Holloway Road, London, N7 8DB.

Infra-Red spectroscopy

Air sensitive IR samples were prepared in the glove box as pressed KBr discs. Spectra were recorded on a Nicolet iS5 ThermoScientific spectrometer in transmission mode (range 4000-400 cm^{-1}, resolution 1 cm^{-1}).

Gas chromatography-mass spectrometry (GC-MS)

GC-MS were recorded on an Agilent Technologies 7820A GC system equipped with a PLOT column (27.5 m x 0.32 mm x 5 µm), coupled to an Agilent Technologies 5977E MSD instrument.

Solid state NMR spectroscopy

Samples were prepared in the glovebox and packed in 4 mm ZrO_2 rotors. Solid state ^{13}C and ^{27}Al NMR spectra were recorded by Dr. Nicholas H. Rees, University of Oxford, on a Bruker AVIII HD NanoBay 400 MHz Solid-State NMR spectrometer. Samples were spun at the magic angle (54.71°) at a spin rate of 10 kHz (^{13}C CPMAS) or 15 kHz (^{27}Al DPMAS). ^{13}C NMR spectra were referenced to adamantane and ^{27}Al to $Al(NO_3)_3$.

Complex synthesis

$W(NDipp)Cl_4(L)$ (L = THF or Et_2O) was synthesized according to a literature procedure.[1]

$W(NDipp)Me_3Cl$ (Dipp = 2,6-^{i}Pr-C_6H_3) $W(NDipp)Cl_4(Et_2O)$ (500 mg, 0.87 mmol) and trimethylaluminium (TMA) (62.7 mg, 0.87 mmol) were dissolved in benzene (~20 mL) and the TMA solution added dropwise to the green $W(NDipp)Cl_4(Et_2O)$ solution. This led to an immediate colour to dark orange/brown. The solvent was reduced *in vacuo* and the resulting brown solid dissolved in hexane to yield an orange solution. This was filtered, reduced to minimum volume and cooled to –30 °C, resulting in orange crystals (300 mg) that were suitable for a single crystal X-ray diffraction study and shown to be $W(NDipp)Me_3Cl$. Yield 79%. ^1H NMR (C_6D_6) δ (ppm):

7.04 (d, 2H, Ar**H**$_{meta}$), 6.97 (dd, 1H, Ar**H**$_{para}$), 3.53 (sept, 2H, ArC**H**$(CH_3)_2$), 1.41 (s, 9H, W(C**H$_3$**)$_3$, $^2J_{WH}$ = 7.027 Hz), 1.08 (d, 12H, ArCH(C**H**$_3)_2$). $^{13}C\{^1H\}$ NMR (C_6D_6) δ (ppm): 150.42 (**Ar**$_{ipso}$N), 128.3 (**Ar**$_{meta}$H), 128.13 (**Ar**CH$(CH_3)_2$), 123.22 (**Ar**$_{para}$H), 56.54 (W(**C**$H_3)_3$, $^1J_{WC}$ = 156 Hz), 28.83 (Ar**C**H$(CH_3)_2$), 24.28 (ArCH(**C**$H_3)_2$). Elemental analysis (CHN) (%): Expected C 40.98, H 5.96, N 3.19. Found C 40.92, H 5.88, N 3.18.

W(NDipp)Me$_4$ W(NDipp)Me_3Cl (10 mg, 0.02 mmol) was charged in a Young's tap NMR tube and dissolved in C_4D_8O. MeLi (1.6 M in Et_2O, 14.4 µL, 0.02 mmol) was added *via* syringe and the contents mixed. An immediate colour change from orange to yellow was observed before fast decomposition which yielded a dark solid. ^{1}H NMR spectroscopy displayed no resonances corresponding to an imido complex.

General supporting procedure

Layered Double Hydroxides (LDHs) of the type Mg_3AlX where $[Mg_{0.75}Al_{0.25}(OH)_2](X^{n-})_{0.25/n}$ (X = CO_3, NO_3 and SO_4) were prepared by the aqueous miscible organic solvent treatment method (AMOST),[2–4] and were thermally treated at 150 °C for 6 h under vacuum prior to use. LDH-MAO was prepared by reacting 2 equivalents of LDH to one equivalent of MAO in toluene at 80 °C for 2 hours. The resulting suspension was filtered and dried to yield a white solid. Polymethylaluminoxane was synthesised according to a literature procedure.[5]

5% W(NDipp)$Cl_4(Et_2O)$ by weight was reacted with the chosen support in toluene. For example W(NDipp)$Cl_4(Et_2O)$ (10 mg, 17.4 µmol), and Mg_3AlSO_4 (200 mg) were charged in separate schlenks. Toluene (~20 ml) was added to both and the green complex solution filtered across. The resulting suspension was swirled intermittently for one hour. Immediate decolouration of the green solution was observed and the colourless support became orange. After one hour the solution was completely clear and colourless at which point it was filtered off. The remaining solid was washed with pentane (2 x 20 mL) and dried *in vacuo* to yield a beige solid in near quantitative yield. The colour of the support varied dependent on the solid used; both silica and Mg_3AlCO_3 yielded beige powders, whereas Mg_3AlSO_4 was off-white, Mg_3AlNO_3 bright yellow and the LDHMAO and polymethylaluminoxane supported complexes pale yellow.

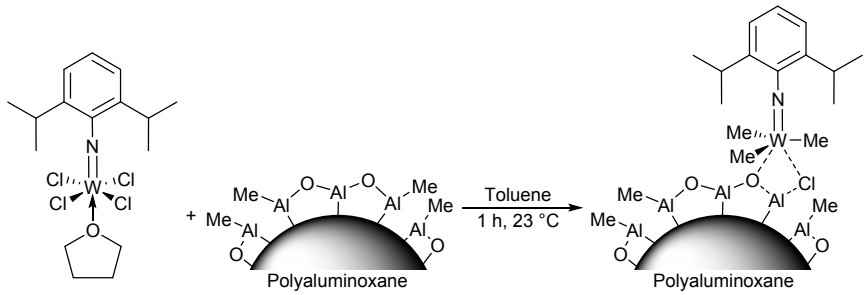

Scheme S1. Supporting of W(NDipp)Cl_4(THF) on polymethylaluminoxane resulting in methylation of the complex on the surface.

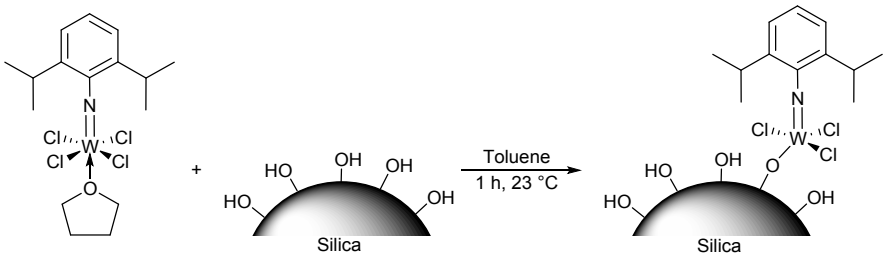

Scheme S2. Supporting of W(NDipp)Cl_4(THF) on silica.

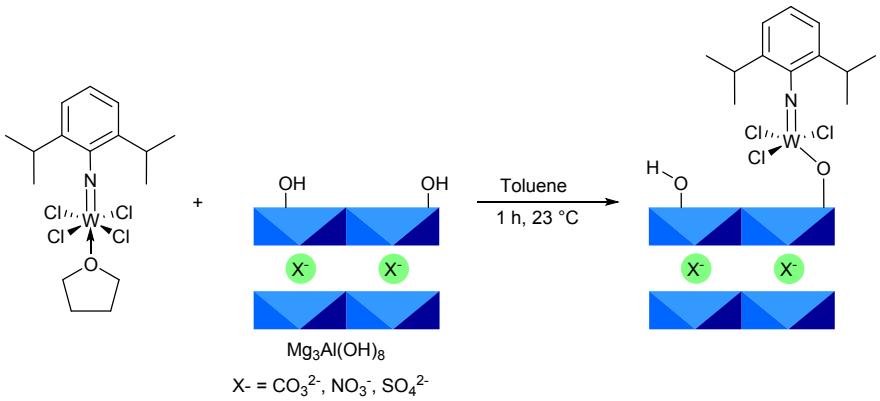

Scheme S3. Supporting of W(NDipp)Cl_4(THF) on Mg_3Al- SO_4, NO_3 and CO_3 LDHs.

W(NDipp)Me_3Cl was also supported on polymethylaluminoxane in toluene yielding a colourless solution and yellow solid. Filtering and drying left a pale yellow solid.

General oligomerisation procedure

All oligomerisation reactions were performed in oven-dried Young's taps NMR tubes which were loaded in the glovebox, degassed and ethylene added *via* a vacuum/nitrogen/ethylene manifold. An internal standard stock solution was made by adding pyridine (10 µL, 124 µmol) to C_6D_6 (240 µL) using a microlitre syringe. 20 µL of stock solution (9.93 µmol pyridine) was added to each NMR tube prior addition of ethylene. For supported complexes where the support was not either composed of MAO or the surface had not been contacted with MAO prior to supporting, MAO (2 mg, W:MAO = 1:40) was added prior to starting the run. Runs were periodically analysed by ^{1}H NMR spectroscopy and once stopped by GC-MS.

Homogenous oligomerisation

W(NDipp)Me_3Cl (2 mg, 4.55 µmol) and MAO (W:MAO = 1:2, 1:5, 1:10 and 1:20) were added to a Young's tap NMR tube and dissolved in C_6D_6 (500 mg). The internal standard was added and the solution freeze-pump-thaw degassed three times. Ethylene (1 bar) was added and the tube heated at 100 °C. Formation of 1-butene was observed by ^{1}H NMR spectroscopy along with some isomerisation to 2-butenes and a small amount of propylene as the metathesis product. It should be noted that a small amount of methane was also observed.

Heterogeneous oligomerisation

The supported complex (5 mg) was added to a Young's tap NMR tube, along with MAO if required, and dissolved in C_6D_6 (500 mg). The internal standard was added and the tube freeze-pump-thaw degassed three times. Ethylene (1 bar) was added and the run started.

2. X-ray crystallography

Crystals were mounted on MiTeGen MicroMounts using perfluoropolyether oil and rapidly transferred to a goniometer head on a diffractometer fitted with an Oxford Cryosystems Cryostream open-flow nitrogen

cooling device.[6] Data collections were carried out at 150 K on an Enraf-Nonius FR590 KappaCCD diffractometer, utilising graphite-monochromated Mo Kα X-ray radiation (λ = 0.71073 Å). Intensity data were processed using the DENZO-SMN package[7] and corrected for absorption using SORTAV.[8] The structure was solved using a charge flipping algorithm (SUPERFLIP)[9] and refined by full-matrix least-squares using CRYSTALS[10,11] or the Win-GX software suite.[12] Illustration of the solid state molecular structure was created using ORTEP.[13] Interplanar distances and angles were calculated using PLATON.[14,15]

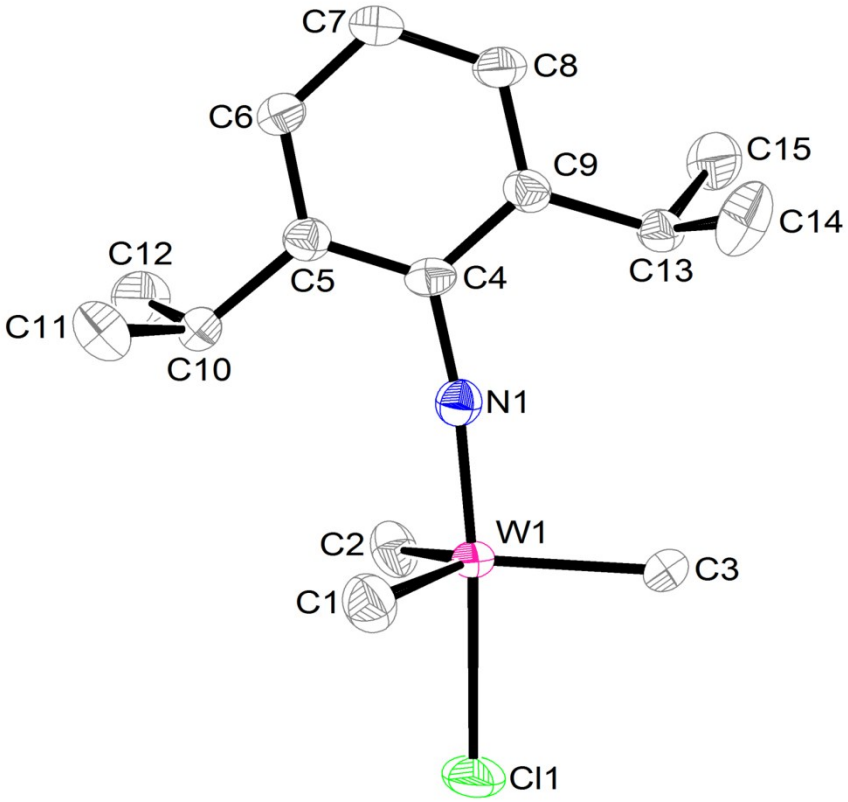

Figure S1. Molecular structure of W(NDipp)Me_3Cl. Thermal ellipsoids shown at 50% probability. Hydrogen atoms omitted for clarity.

Table S1. Selected bond lengths and angles for W(NDipp)Me_3Cl. Numbers in parentheses refer to estimated standard deviations.

Bond	Length (Å)/Angle (°)
W-Me av.	2.1081
W1-N1	1.7370(1)
W1-Cl1	2.4156(1)
W1-N1-C4	172.51
Cl1-W1-N1	174.95
C1-W1-C2	122.76

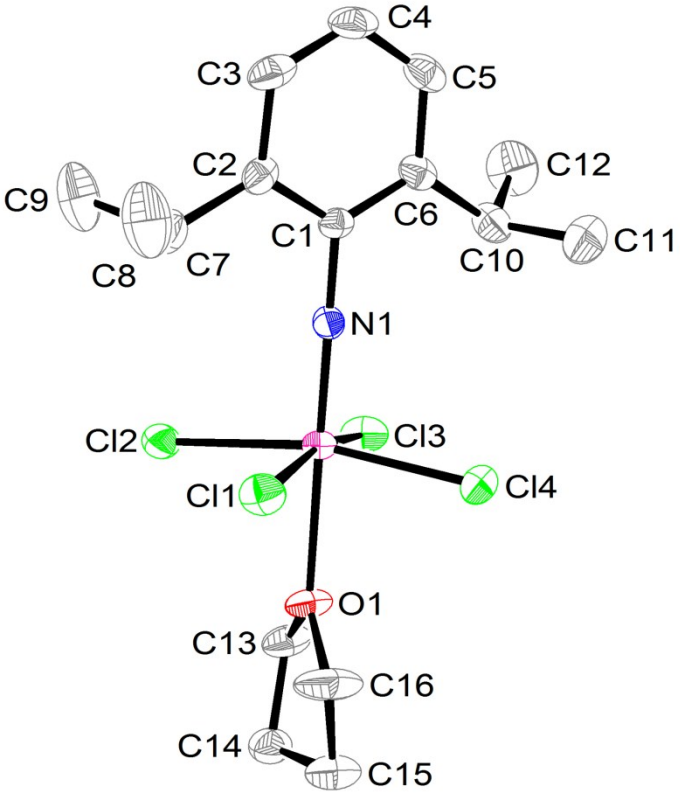

Figure S2. Molecular structure of W(NDipp)Cl_4(THF). Thermal ellipsoids shown at 50%. Hydrogen atoms omitted for clarity.

Table S2. Selected bond lengths (Å) and angles (°) for W(NDipp)Cl_4(THF).

Bond	Length (Å)/Angle (°)
W-Cl av.	2.3348
W1-N1	1.7226(1)
W1-O1	2.2549(1)
W1-N1-C1	178.38(1)
O1-W1-N1	179.27(1)
Cl1-W1-Cl2	167.22(1)

Table S3. Selected experimental crystallographic data.

Crystal data		
CCDC number	1434396	1434397
Chemical formula	$C_{15}H_{26}ClNW$	$C_{16}H_{25}Cl_4NOW$
Mr	439.67	573.02
Crystal system, space group	Orthorhombic, *Pna*2_1	Triclinic, $P\bar{1}$
Temperature (K)	150	150
***a, b, c* (Å)**	13.1669 (1), 12.7572 (1), 20.0394 (2)	8.5941 (1), 14.1186 (2), 17.4478 (3)
α, β, γ (°)	90	95.806 (1), 98.562 (1), 97.484 (1)
***V* (Å^3)**	3366.07 (5)	2059.88 (5)
Z	8	4
m (mm^{-1})	7.01	6.13
Crystal size (mm)	0.22 × 0.20 × 0.18	0.56 × 0.48 × 0.14
Data collection		
Diffractometer	Nonius KappaCCD diffractometer	Nonius KappaCCD diffractometer
Absorption correction	Multi-scan *DENZO/SCALEPACK* (Otwinowski & Minor, 1997)	Multi-scan *DENZO/SCALEPACK* (Otwinowski & Minor, 1997)
***T*$_{min}$, *T*$_{max}$**	0.75, 1.00	0.76, 1.00
No. of measured, independent and observed [*I* > 2*s*(*I*)] reflections	64889, 7358, 6627	17151, 9396, 7987
***R*$_{int}$**	-	0.029
(sin q/l)$_{max}$ (Å^{-1})	0.650	0.650
Refinement		
R*[*F*^{2} > 2*s*(*F*^{2})], *wR*(*F*^{2}), *S	0.030, 0.073, 0.96	0.029, 0.069, 1.10
No. of reflections	7358	9396
No. of parameters	340	433
No. of restraints	1	1
H-atom treatment	H-atom parameters constrained	H-atom parameters constrained
(Δ/σ)$_{max}$	0.001	0.002
Δρ$_{max}$, Δρ$_{min}$ (e Å^{-3})	1.93, -1.79	1.66, -1.52
Absolute structure	Refined as an inversion twin.	-
Absolute structure parameter	0.495 (16)	-

Computer programs: Collect (Nonius BV, 1997-2000), *HKL SCALEPACK* (Otwinowski & Minor 1997), *HKL DENZO* and *SCALEPACK* (Otwinowski & Minor 1997), Palatinus, L.; Chapuis, G. J. Appl. Cryst. 2007, 40, 786-790., *SHELXL2014* (Sheldrick, 2014), *ORTEP-3 for Windows* (Farrugia, 1997), *WinGX* publication routines (Farrugia, 1999).

3. DFT computational studies

All DFT calculations were performed with the ORCA program package.[16] The geometry optimizations of the complexes and single-point calculations on the optimized geometries were carried out at the BP86[17–19] level of DFT. Relativistic effects were accounted for by including the zeroth-order regular approximation (ZORA).[20–22] The def2-TZVP(-f) basis set in the scalar relativistic recontraction reported by Neese *et al.* (segmented all-electron relativistic basis sets, SARC) was applied.[23,24] For all elements up to bromine, the SARC basis sets are simply scalar relativistic recontractions of the basis sets developed by the Karlsruhe group,[25,26] while for heavier elements, the primitives and contraction patterns were designed in references 23 and 24. The Coulomb fitting basis set of Weigend[27] was used in uncontracted form in all calculations. The RI[28–30] approximation was used to accelerate the calculations. Orbitals were generated with the program Chimera.[31]

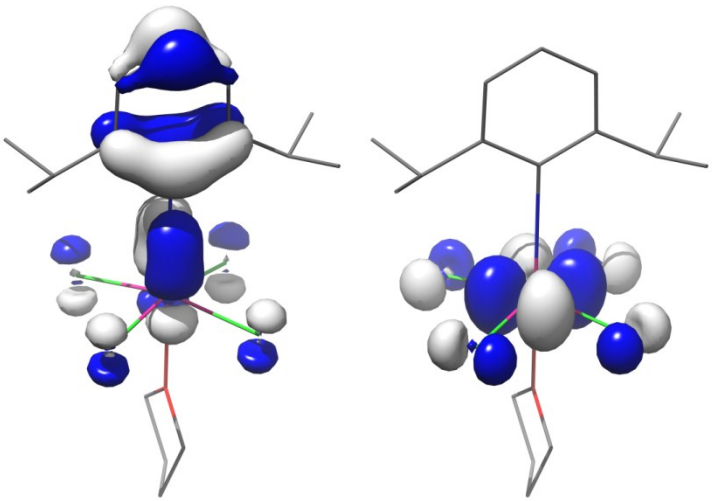

Figure S3. DFT-computed (BP86) HOMO (left) and LUMO (right) W(NDipp)Cl_4(THF).

Table S4. Comparison of selected calculated and experimental bond lengths (Å) and angles (°) for W(NDipp)Cl_4(THF).

Bond	Experimental	Calculated – BP86
W-Cl av.	2.3348	2.3525
W1-N1	1.7226(1)	1.749
W1-O1	2.2549(1)	2.334
W1-N1-C1	178.38(1)	179.76
O1-W1-N1	179.27(1)	179.92
Cl1-W1-Cl2	167.22(1)	165.60

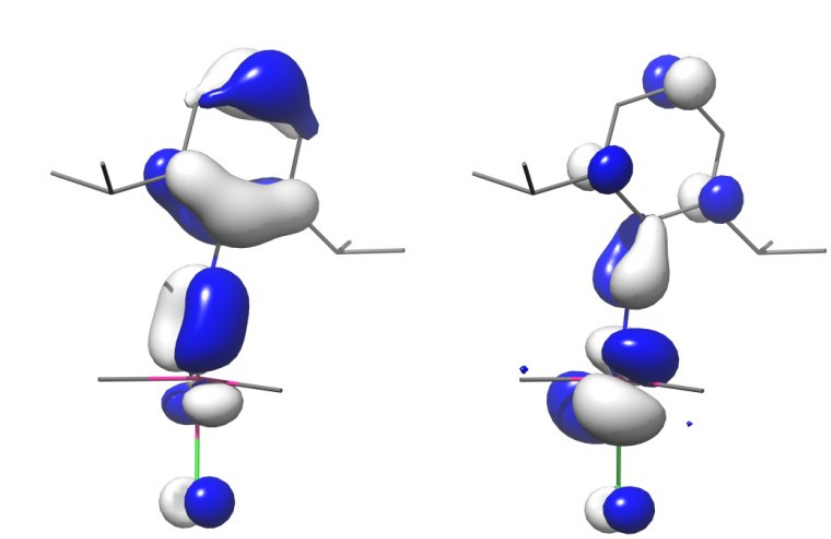

Figure S4. DFT-computed (BP86) HOMO (left) and LUMO (right) W(NDipp)Me_3Cl.

Table S5. Comparison of selected calculated and experimental bond lengths (Å) and angles (°) for W(NDipp)Me_3Cl.

Bond	Experimental	Calculated – BP86
W-Me av.	2.1081	2.214
W1-N1	1.7370(1)	1.775
W1-Cl1	2.4156(1)	2.400
W1-N1-C4	172.51	172.06
Cl1-W1-N1	174.95	174.02
C1-W1-C2	122.76	122.54

4. Homogeneous oligomerisation studies

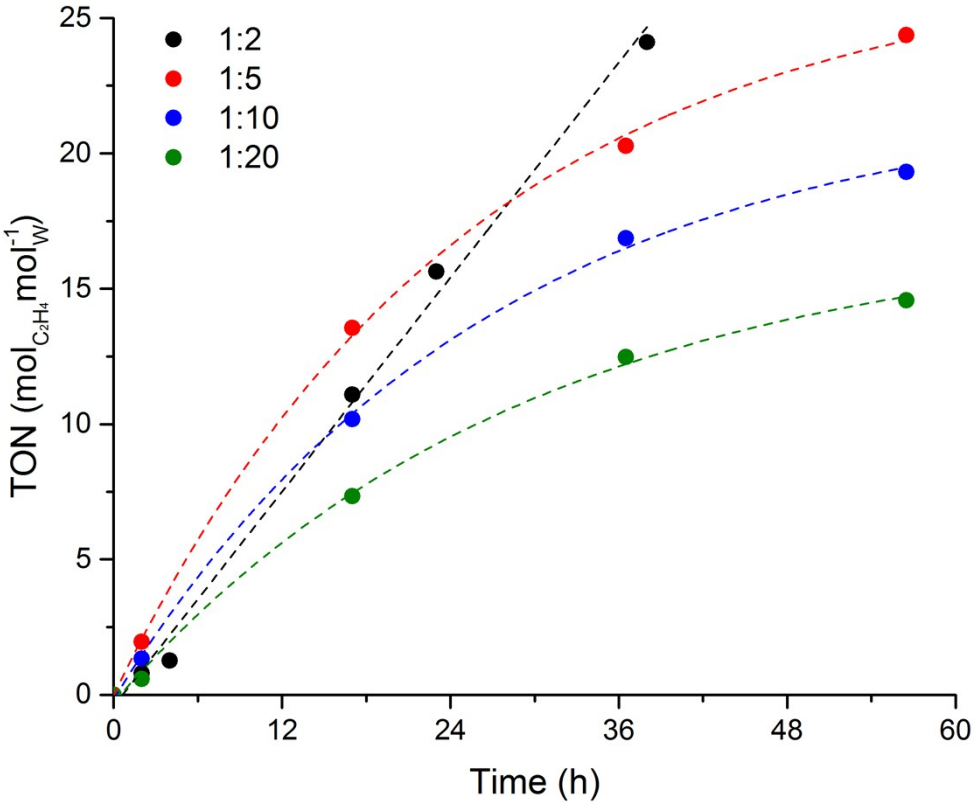

Figure S5. Turnover number (TON) over time for the varying W:MAO ratios. [W(NDipp)Me_3Cl] = 4.55 µmol.

Table S6. Turnover number (TON) for the varying W:MAO ratios over time

Time/h	1:2 TON/mol$_{C_2H_4}$mol$_W^{-1}$h^{-1}	1:5 TON/mol$_{C_2H_4}$mol$_W^{-1}$h^{-1}	1:10 TON/mol$_{C_2H_4}$mol$_W^{-1}$h^{-1}	1:20 TON/mol$_{C_2H_4}$mol$_W^{-1}$h^{-1}
0	0	0	0	0
2	0.79	1.96	1.33	0.59
4	1.27	-	-	-
17	11.09	13.55	10.18	7.33
23	15.64	-	-	-
36.5	-	20.28	16.86	12.48
38	24.11	-	-	-
56.5	-	24.37	19.31	14.58

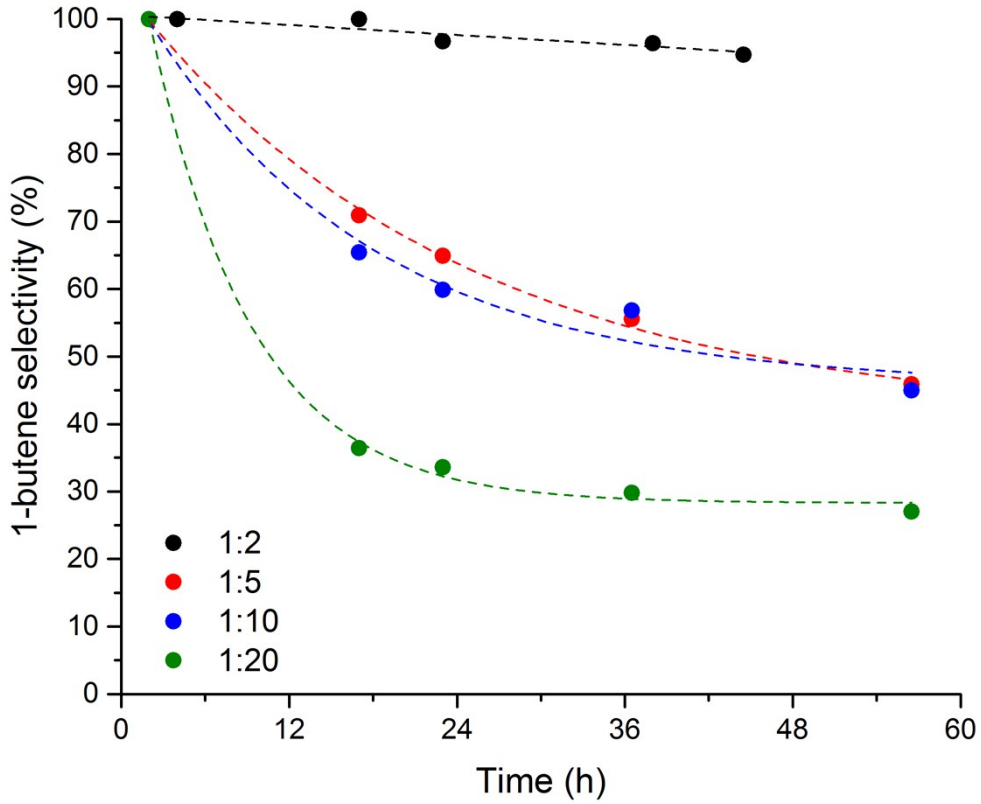

Figure S6. Percentage selectivity for 1-butene over time for the varying W:MAO ratios. [W(NDipp)Me_3Cl] = 4.55 µmol.

Table S7. 1-butene selectivity for the varying W:MAO ratios.

Time/h	1:2 1-butene selectivity/%	1:5 1-butene selectivity/%	1:10 1-butene selectivity/%	1:20 1-butene selectivity/%
2	100	100	100	100
4	100	-	-	-
17	100	70.9	65.4	36.4
23	96.7	64.9	59.9	33.6
36.5	-	55.6	56.8	29.8
38	96.4	-	-	-
44.5	94.7	-	-	-
56.5	-	45.9	45	27

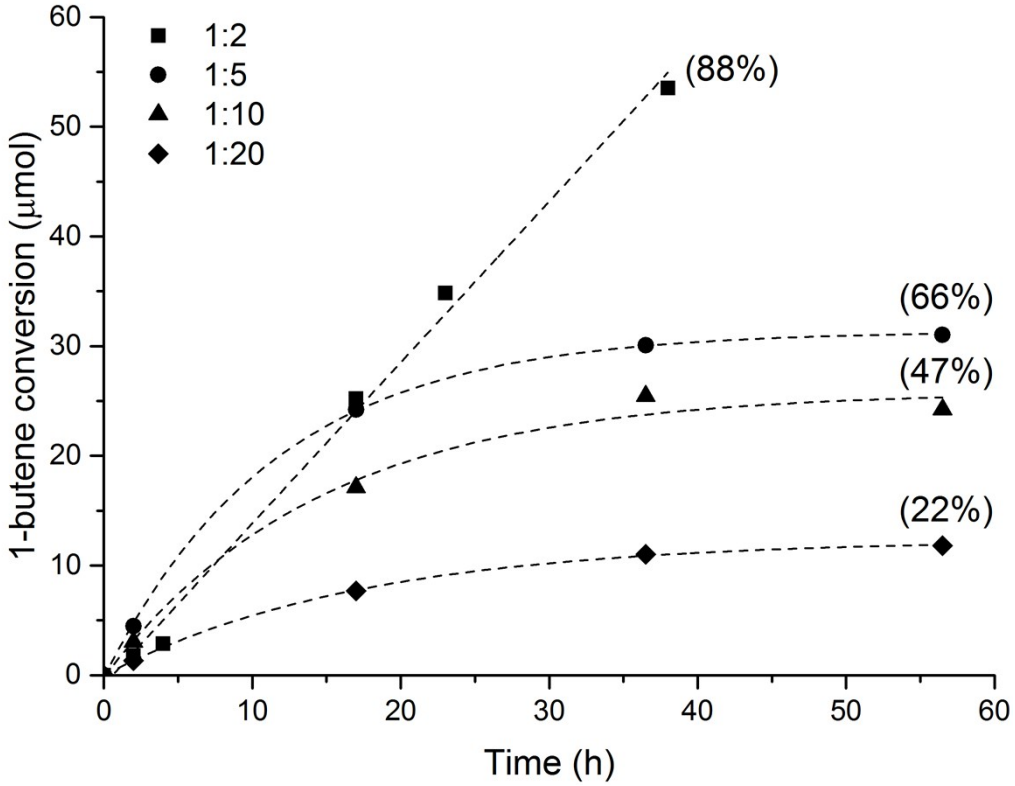

Figure S7. Conversion of ethylene to 1-butene for varying W:Al ratios. Numbers in parentheses correspond to the ethylene conversion at the final data point.

Table S8. Production of 1-butene for the varying W:MAO ratios.

Time/h	1:2 1-butene/µmol	1:5 1-butene/µmol	1:10 1-butene/µmol	1:20 1-Butene/µmol
0	0	0	0	0
2	1.79	4.47	3.03	1.34
4	2.88	--	--	--
17	25.22	24.22	17.12	7.7
23	34.85	--	--	--
36.5	--	30.09	25.46	11.03
38	53.52	--	--	--

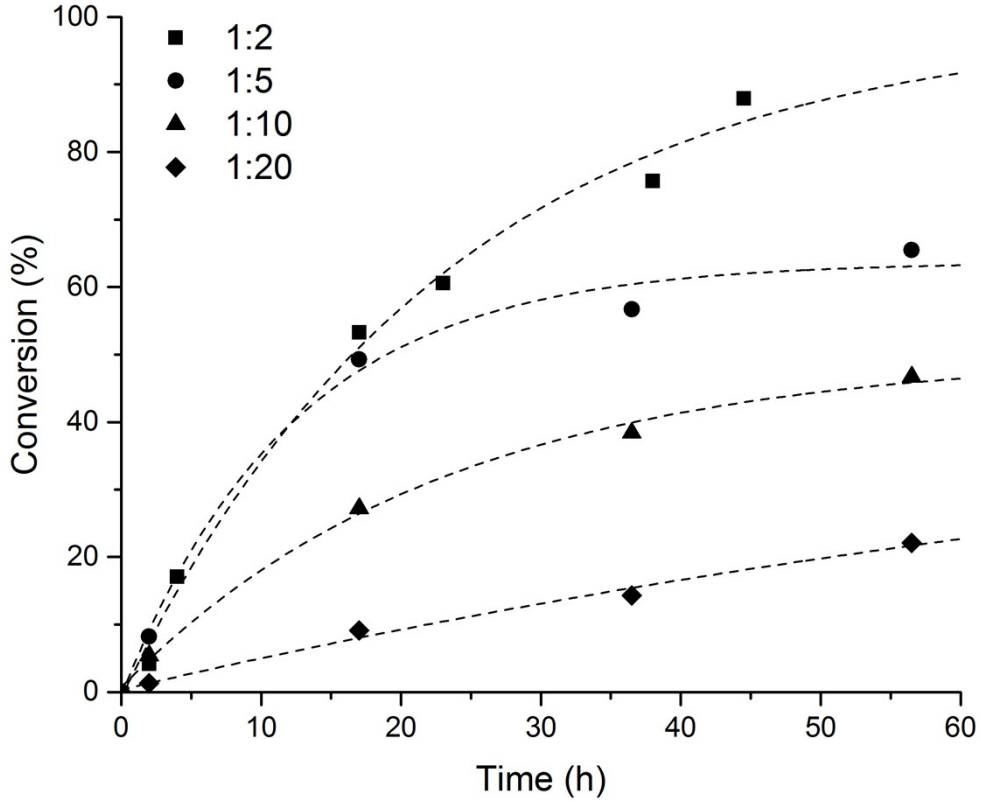

Figure S8. Percentage conversion of ethylene for varying W:MAO ratios.

Table S9. Conversion of ethylene for the varying W:MAO ratios.

Time/h	1:2 Conversion/%	1:5 Conversion/%	1:10 Conversion/%	1:20 Conversion/%
0	0	0	0	0
2	4.2	8.2	5.4	1.3
4	17.1	-	-	-
17	53.3	49.3	27.2	9.1
23	60.6	-	-	-
36.5	-	56.7	38.4	14.3
38	75.7	-	-	-
44.5	87.9	-	-	-
56.5	-	65.5	46.7	22.1

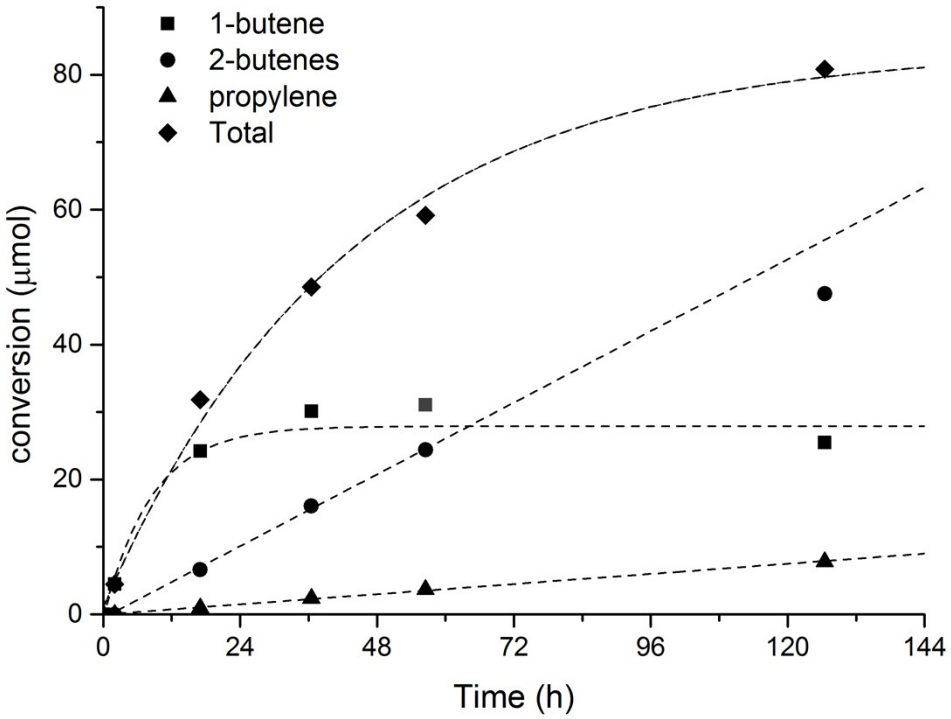

Figure S9. Product composition of the 1:5 ratio over time.

Table S10. Percentage composition of olefinic products for the 1:5 W:MAO ratio.

Time/h	Ethylene/%	1-butene/%	2-butenes/%	Propylene/%	Total (butenes+propylene)/%
0	100	0	0	0	0
2	91.8	8.2	0	0	8.2
17	50.7	37.5	10.3	1.5	49.3
36.5	43.3	35.1	18.7	2.8	56.7
56.5	34.5	34.4	27	4.1	65.5

Table S11. GCMS integrations for the varying W:MAO ratios.

Products	1:5 Peak integration	1:10 Peak integration	1:20 Peak integration
Methane	131394	123398	75712
Ethane	8041	13109	16234
Ethylene	127903	196131	226055
Propylene	166061	25453	10536
Butane	8431	10755	9375
Trans-2-butene	592610	362736	253674
1-butene	1067944	814000	270162
Cis-2-butene	660460	461662	266087

Table S12. Percentage composition of products from GCMS traces for the varying W:MAO ratios.

Products	1:5 % makeup	1:10 % makeup	1:20 % makeup
Methane	4.75	6.15	6.71
Ethane	0.29	0.65	1.44
Ethylene	4.63	9.77	20.04
Propylene	6.01	1.27	0.93
Butane	0.31	0.54	0.83
Trans-2-butene	21.44	18.07	22.49
1-butene	38.64	40.55	23.95
Cis-2-butene	23.90	23.00	23.59

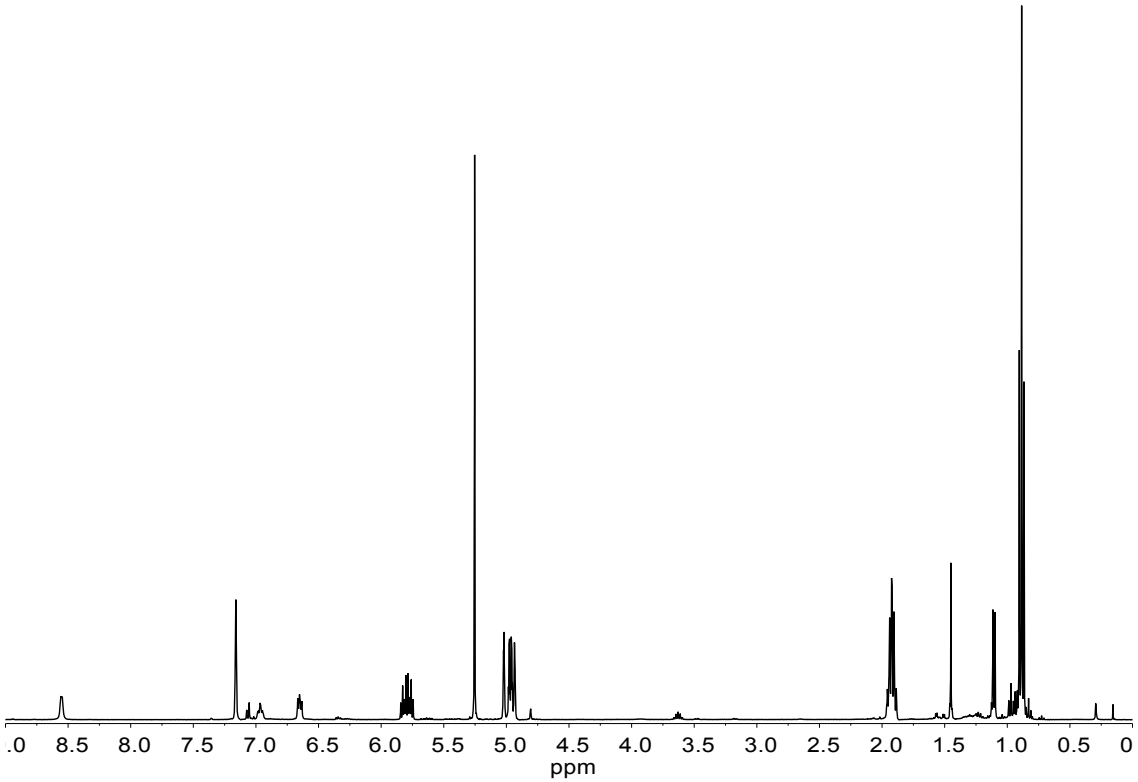

Figure S10. ^{1}H NMR spectrum of the 1:2 W:MAO ratio after 38 h showing resonances for the complex (7.1 3.7, 1.4 and 1.1 ppm), 1-butene (5.6, 5.0, 1.9 and 0.9 ppm), ethylene (5.3 ppm), pyridine (8.6, 7.0 and 6.7 ppm) and C_6D_6 (7.2 ppm).

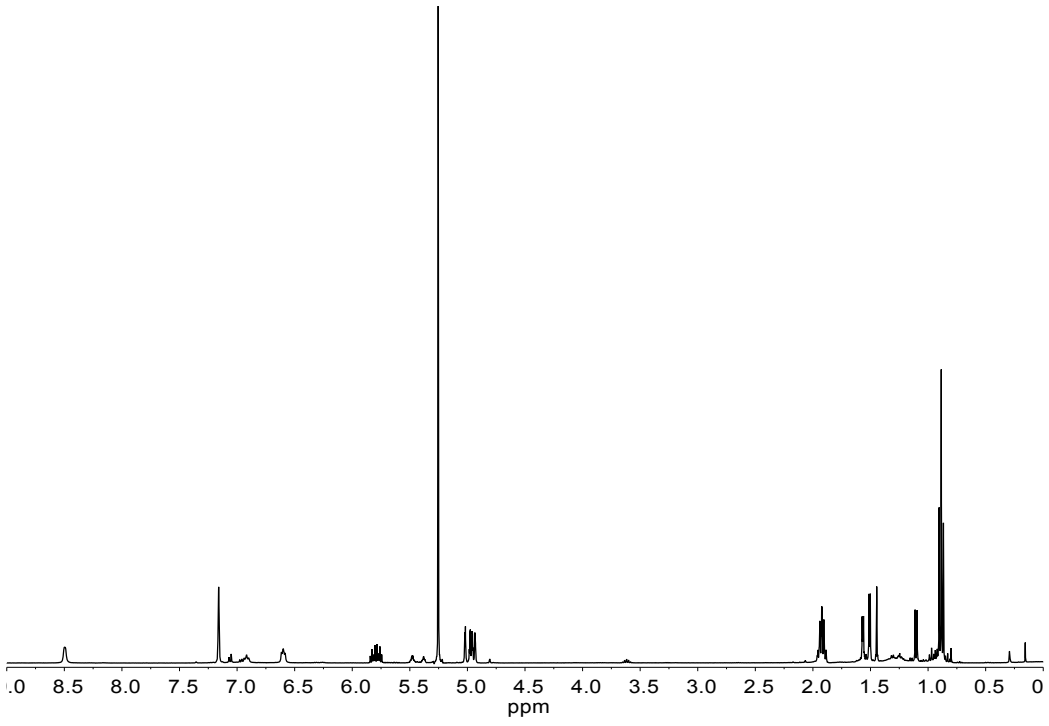

Figure S11. ^{1}H NMR spectrum of the 1:5 after 36.5 h showing resonances for the complex (7.1, 3.7, 1.4 and 1.1 ppm), 1-butene (5.6, 5.0, 1.9 and 0.9 ppm), 2-butenes, propylene, ethylene (5.3 ppm), pyridine (8.6, 7.0 and 6.7 ppm) and C_6D_6 (7.2 ppm).

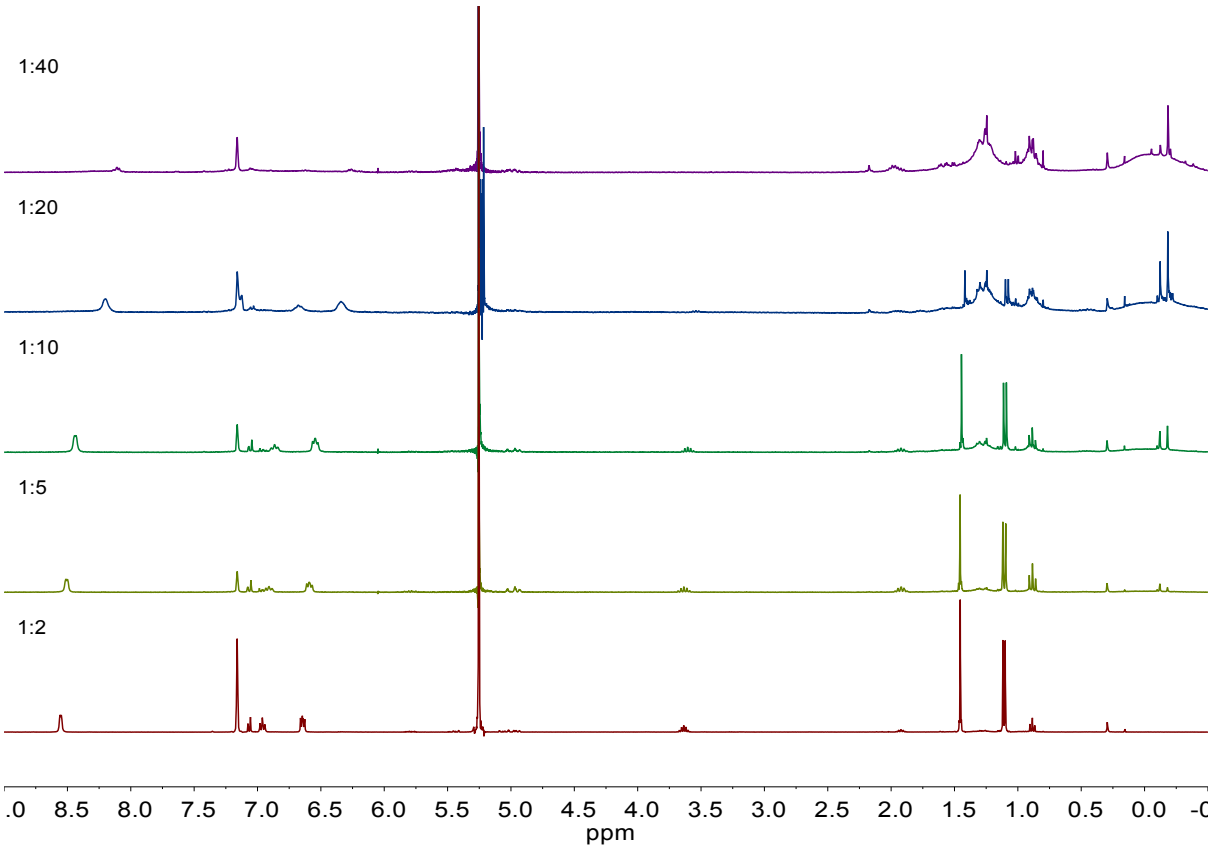

Figure S12. ^{1}H NMR spectra for the homogeneous W:MAO ratios after 2 hours at 100 °C showing decomposition of the complex at higher MAO loadings.

Table S13. 1-butene production for W:DMAC = 1:2 (DMAC = dimethylaluminiumchloride) at 100 °C and 1 bar ethylene in C_6D_6. $[W(NDipp)Me_3Cl]_0$ = 4.55 µmol.

Time/h	1-butene/µmol
1	0.7
17	8.6
23	16.6
46	30.5

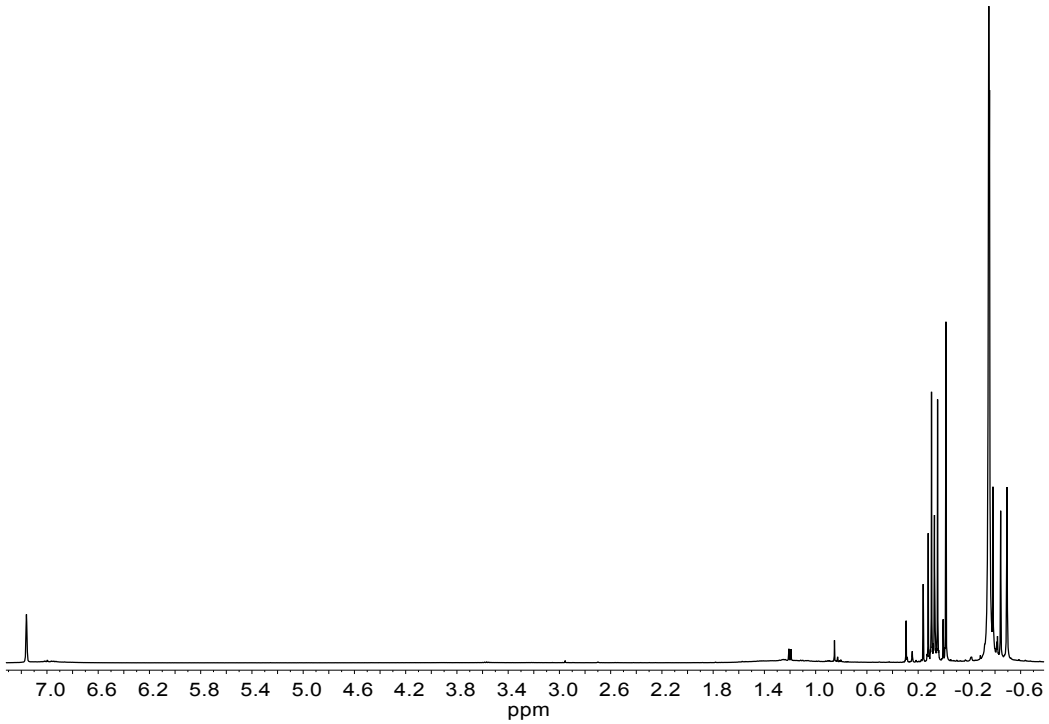

Figure S13. ^{1}H NMR spectrum of the reaction between W(NDipp)Me_3Cl and excess TMA at 100 °C in C_6D_6 resulting in an intractable mixture of products. The resulting species is not reactive towards ethylene.

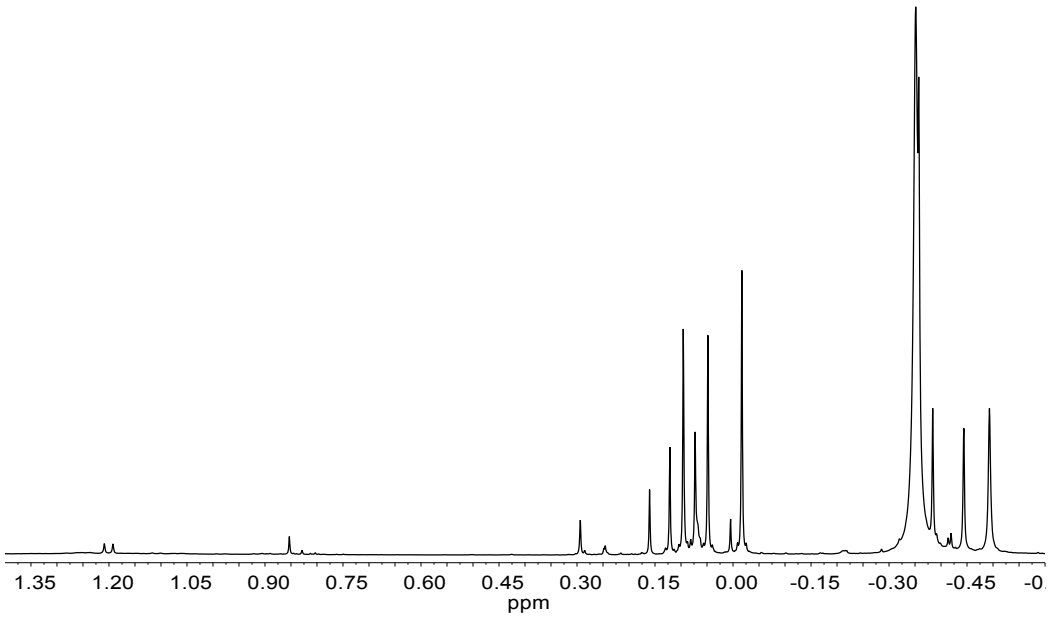

Figure S14. ^{1}H NMR spectrum (Figure S13) between 1.4 and −0.6 ppm showing multiple methyl type resonances with coupling to tungsten.

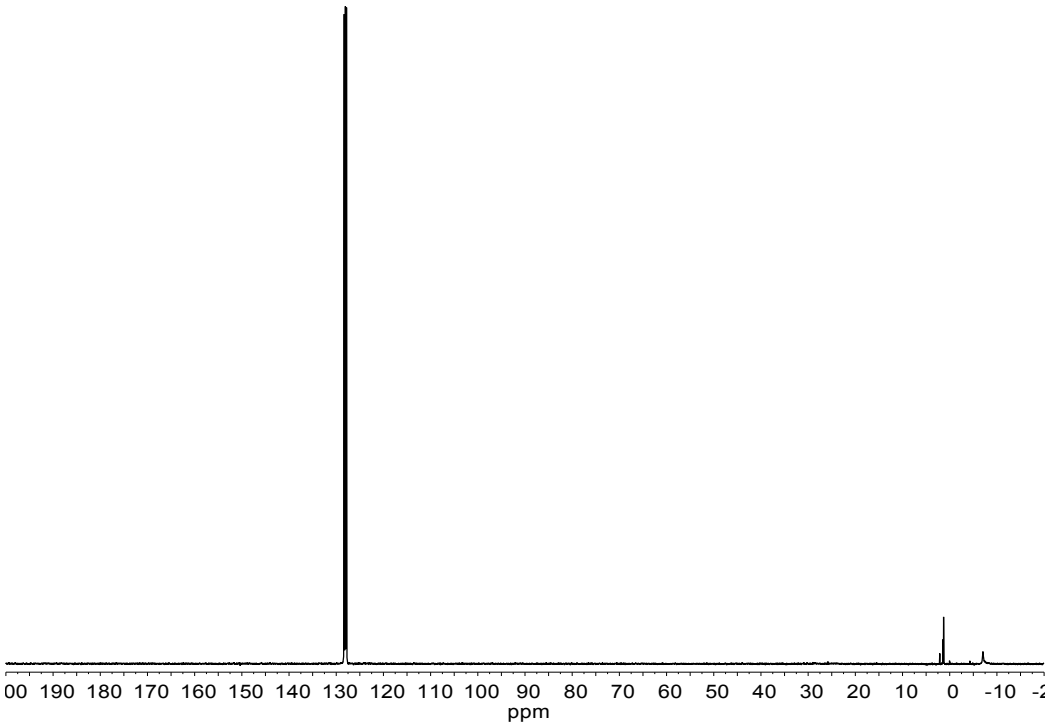

Figure S15. $^{13}C\{^{1}H\}$ NMR spectrum of the reaction between W(NDipp)Me_3Cl and excess TMA at 100 °C in C_6D_6 resulting in an intractable mixture of products. The resulting species is not reactive towards ethylene.

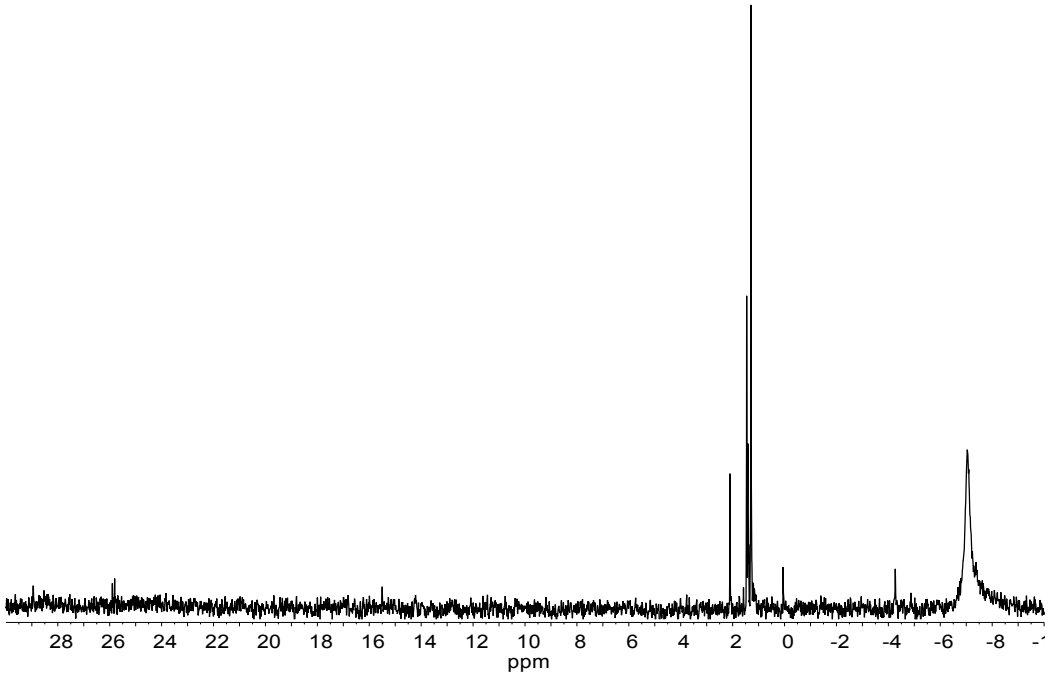

Figure S16. ^{1}H NMR spectrum (Figure S15) zoomed between 30 and −10 ppm.

Postulated metallocycle mechanism

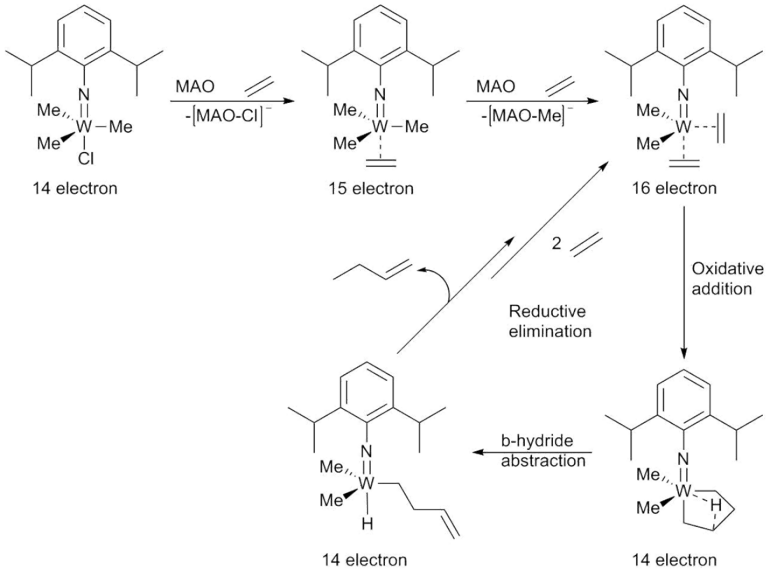

Scheme S4. Postulated metallocyclic mechanism for selective 1-butene formation using W(NDipp)Me_3Cl.

5. Characterisation data for the heterogeneous catalysts

Solid state NMR spectroscopy

The following compounds involve supporting the complex $W(NDipp)Cl_4(Et_2O)$ on the surface of Layered Double Hydroxides and silica resulting in the proposed species $W(NDipp)Cl_3$ being bound to surface oxygen atoms. In the ^{13}C NMR spectral resonances in the region 120-160 ppm correspond to aromatic carbon environments and 10-30 the isopropyl groups. ^{27}Al spectral resonances for LDHs show the bulk aluminium environment (≈ 8 ppm) along with the surface aluminium sites (≈ 77 ppm).

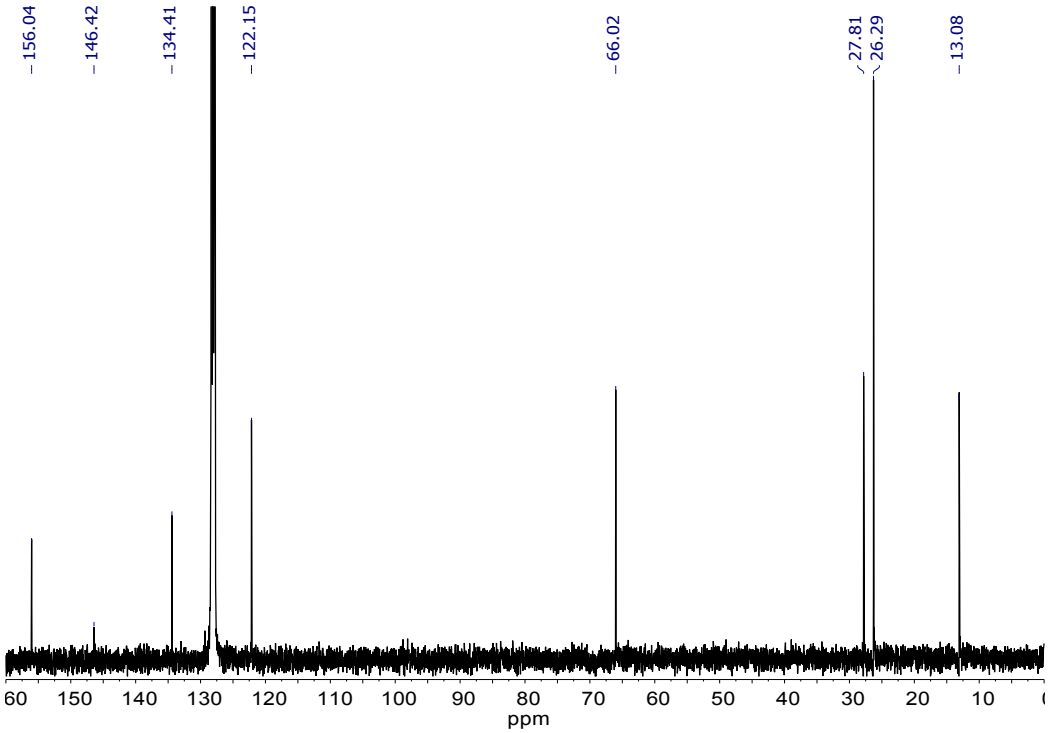

Figure S17. $^{13}C\{^1H\}$ NMR spectrum of $W(NDipp)Cl_4(Et_2O)$ in C_6D_6.

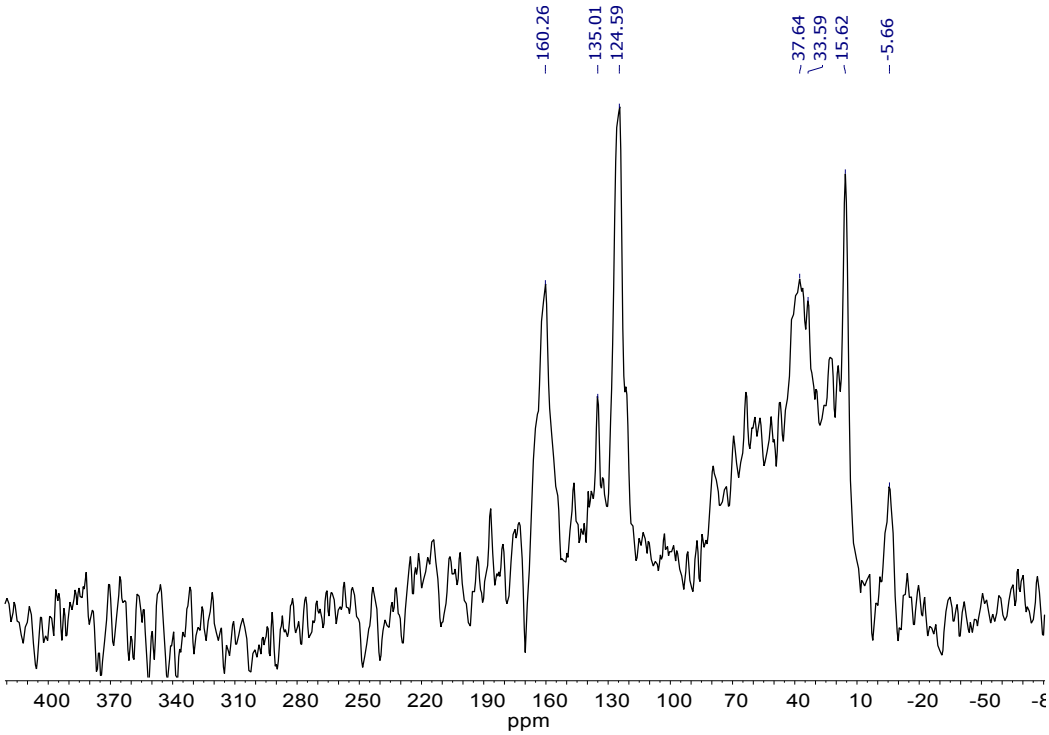

Figure S18. ^{13}C solid state NMR spectrum of Mg_3AlNO_3-W(NDipp)Cl_4.

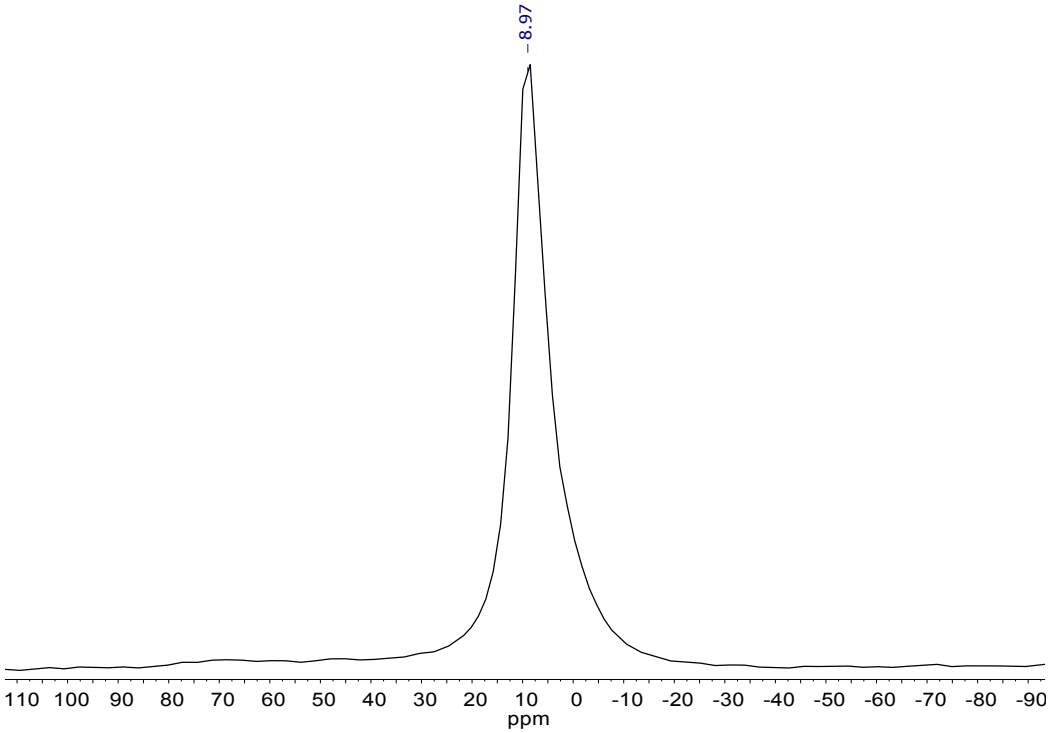

Figure S19. ^{27}Al NMR spectrum of Mg_3AlNO_3-W(NDipp)Cl_4.

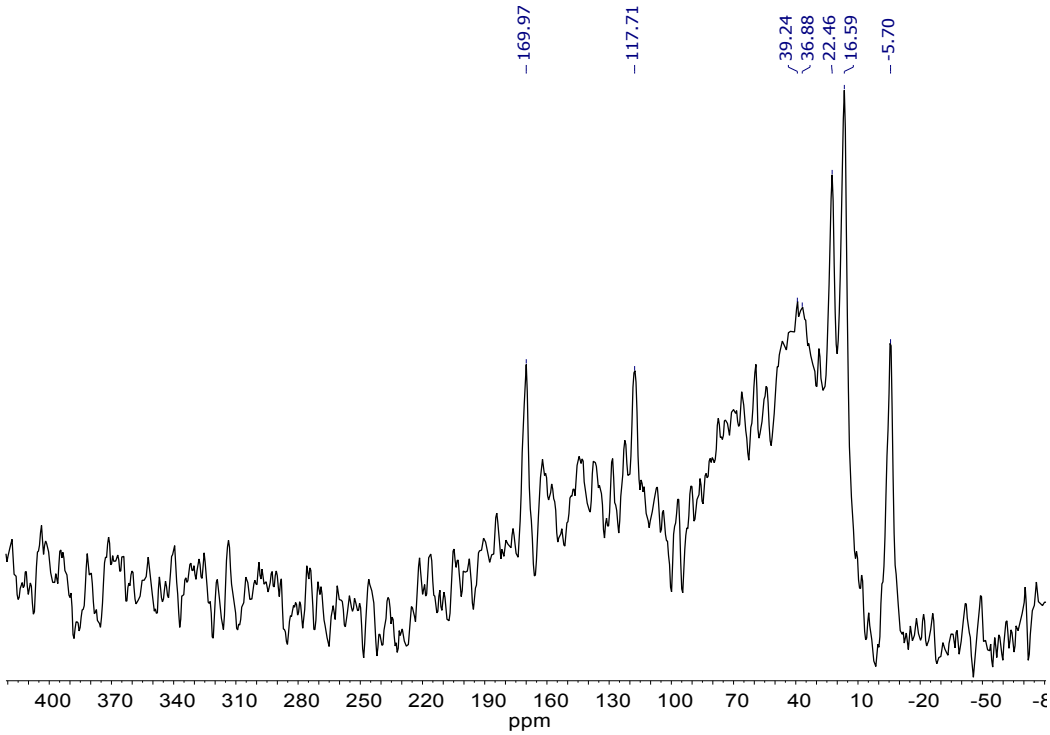

Figure S20. ^{13}C solid state NMR spectrum of SiO_2-W(NDipp)Cl_4(THF).

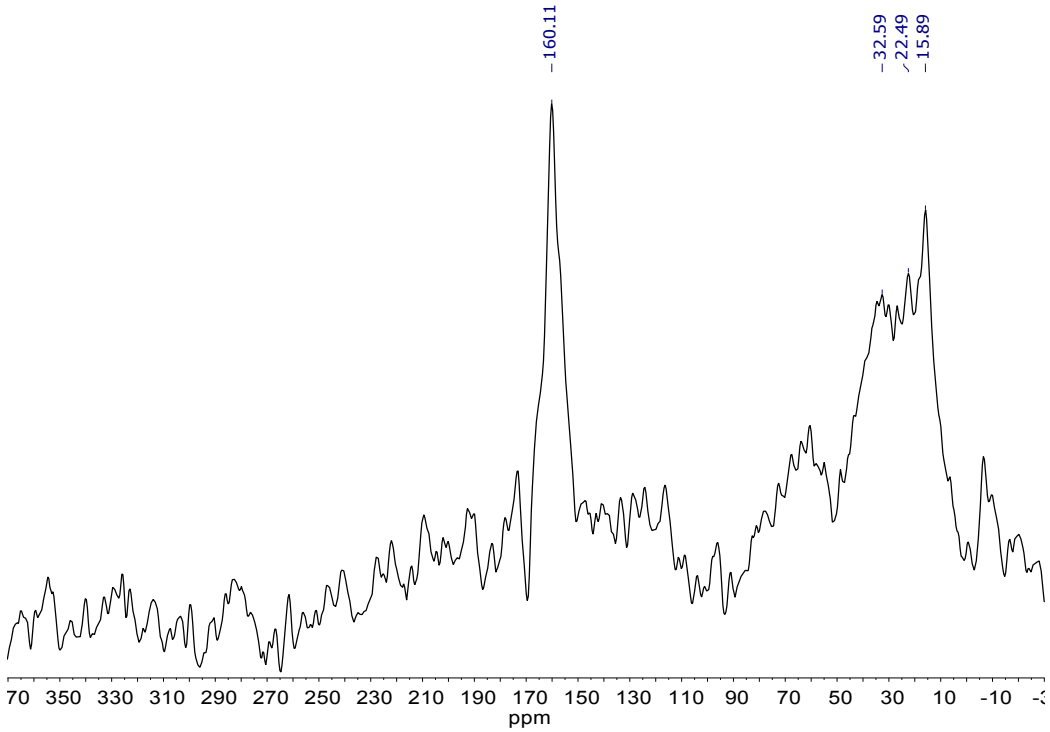

Figure S21. ^{13}C solid state NMR spectrum of Mg_3AlSO_4-W(NDipp)Cl_4(THF).

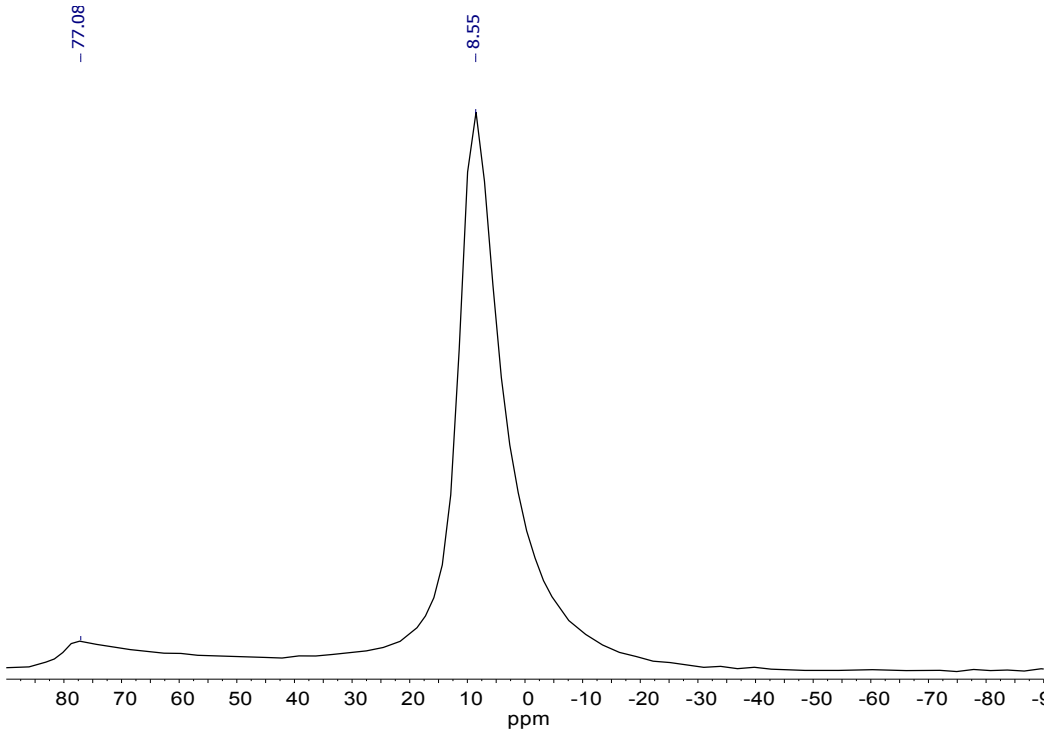

Figure S22. ^{27}Al solid state NMR spectrum of Mg_3AlSO_4-W(NDipp)Cl_4(THF).

The following supported species involve reaction with methylaluminium species and thus the trimethyl complex is postulated to form on the surface. In the ^{13}C NMR spectra, resonances in the region 120-160 ppm correspond to aromatic carbon environments and 10-30 the isopropyl groups. Resonances around 45 ppm correspond to methyls bound to tungsten.

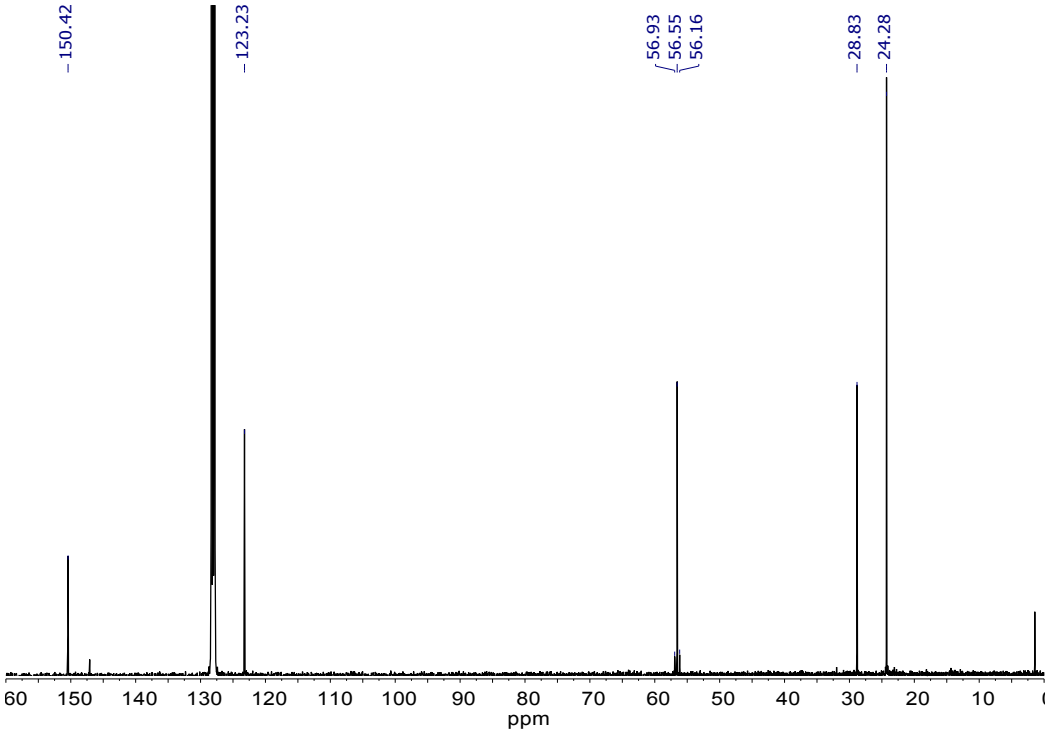

Figure S23. ^{13}C{^{1}H} NMR spectrum of W(NDipp)Me_3Cl in C_6D_6. Resonance at 1.38 ppm corresponds to silicone grease.

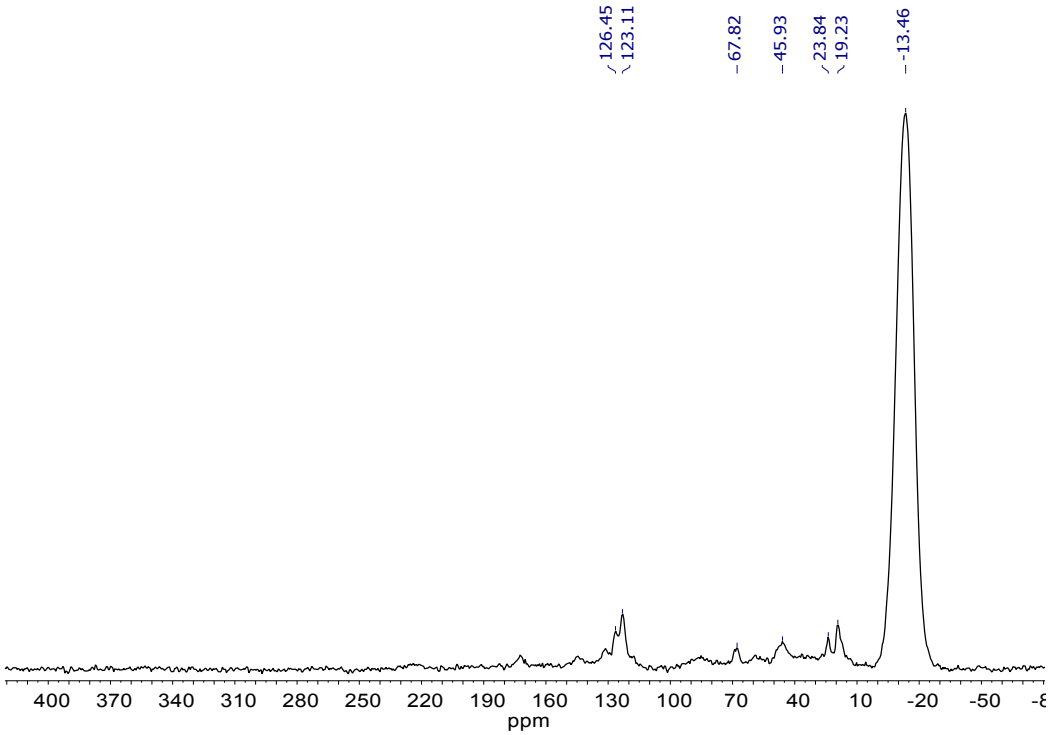

Figure S24. ^{13}C solid state NMR spectrum of polymethylaluminoxane supported W(NDipp)Me_3Cl.

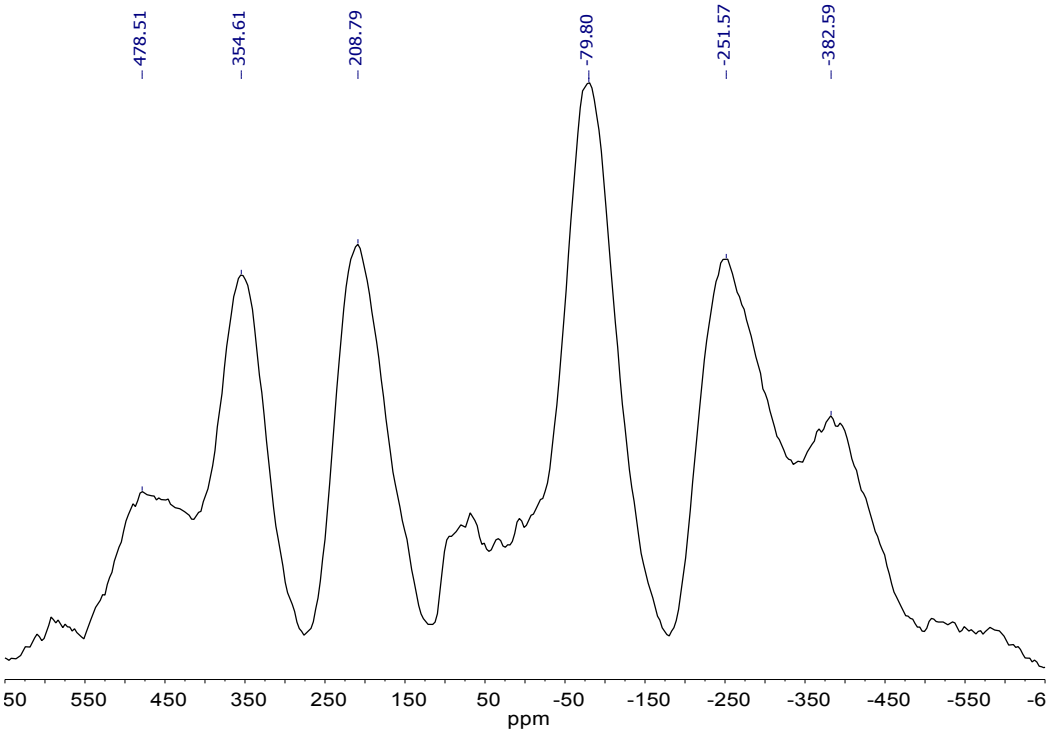

Figure S25. ^{27}Al solid state NMR spectrum of polymethylaluminoxane supported W(NDipp)Me_3Cl.

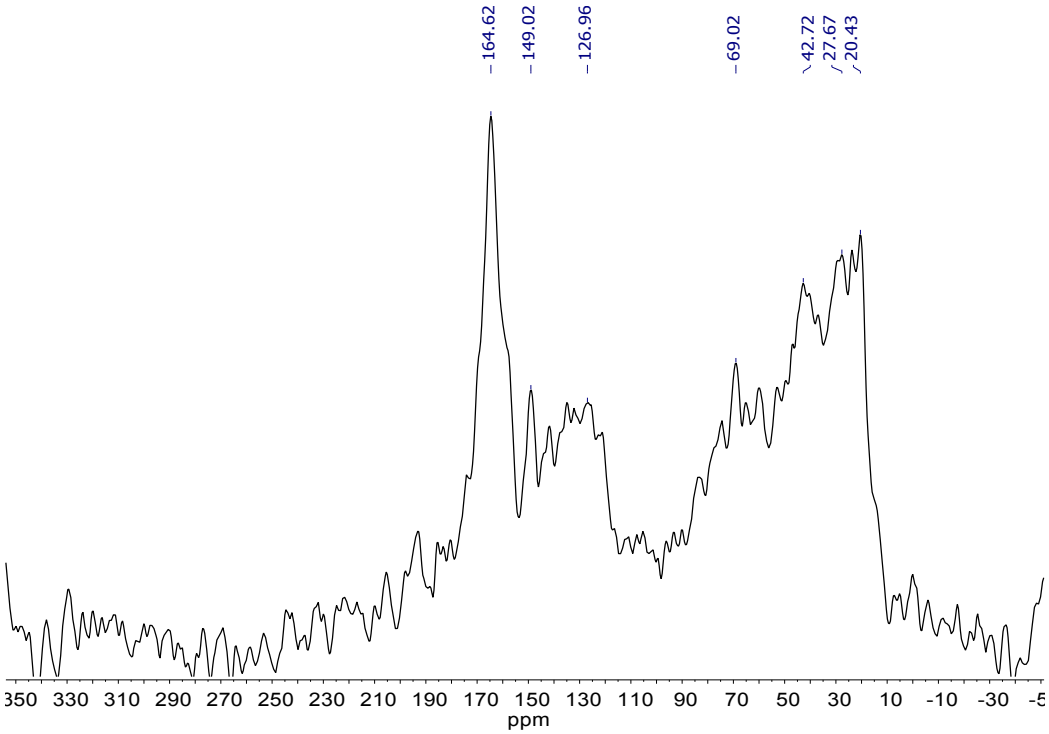

Figure S26. ^{13}C solid state NMR of W(NDipp)Cl_4(THF) supported of Mg_3AlSO_4-MAO.

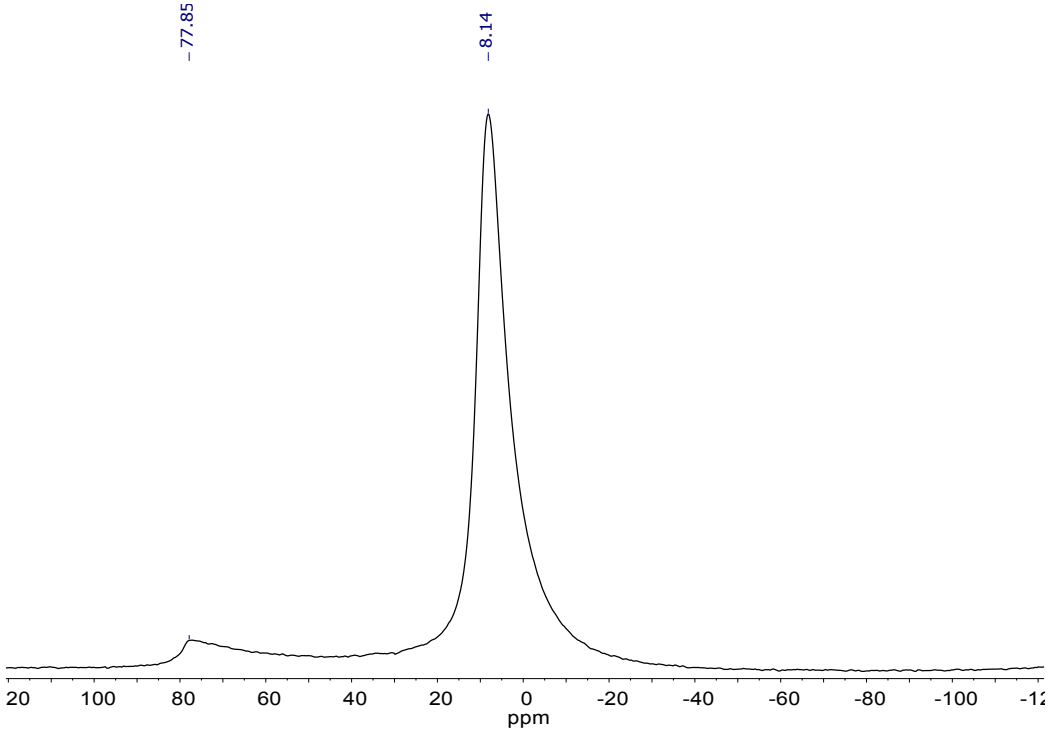

Figure S27. ^{27}Al solid state NMR spectrum of W(NDipp)Cl_4(THF) supported on Mg_3AlSO_4-MAO.

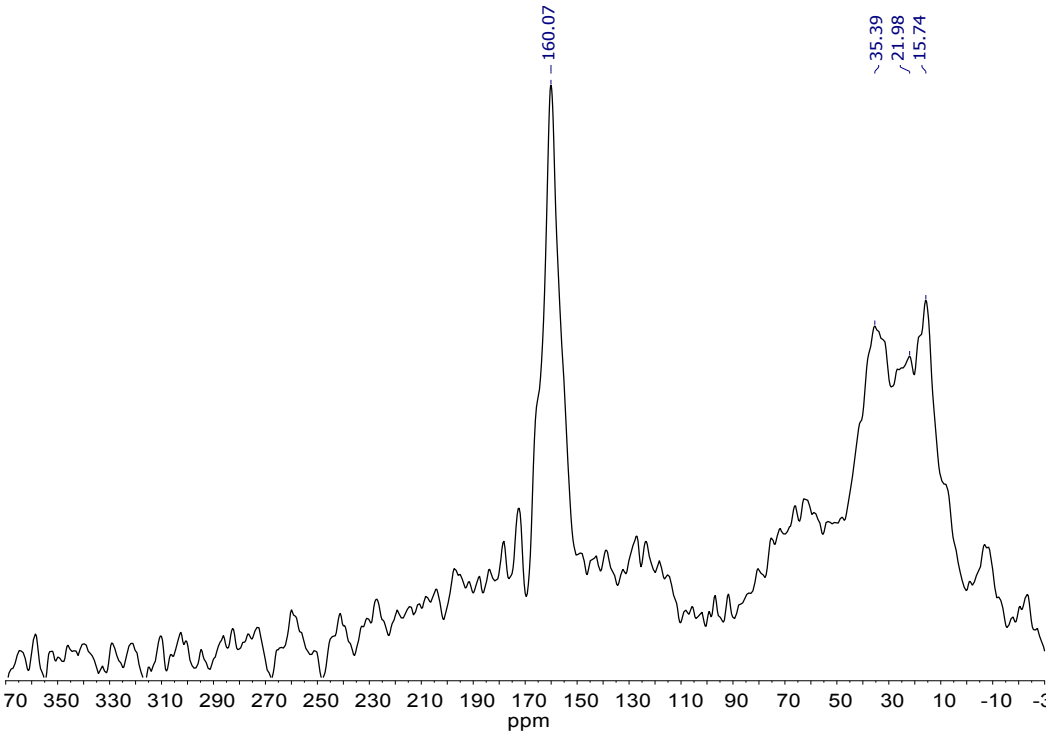

Figure 28. ^{13}C solid state NMR spectrum of W(NDipp)CL_4 contacted with MAO (W:Al = 1:2) prior to immobilisation on Mg_3AlSO_4.

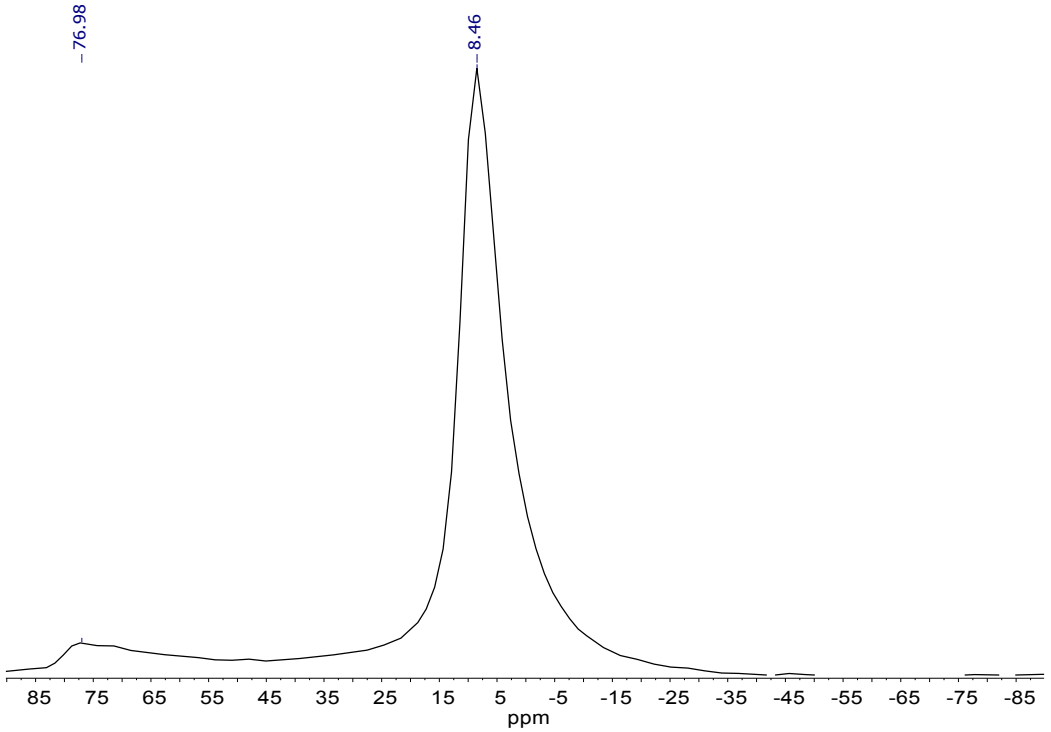

Figure S29. ^{27}Al solid state NMR spectrum of W(NDipp)CL_4 contacted with MAO (W:Al = 1:2) prior to immobilisation on Mg_3AlSO_4.

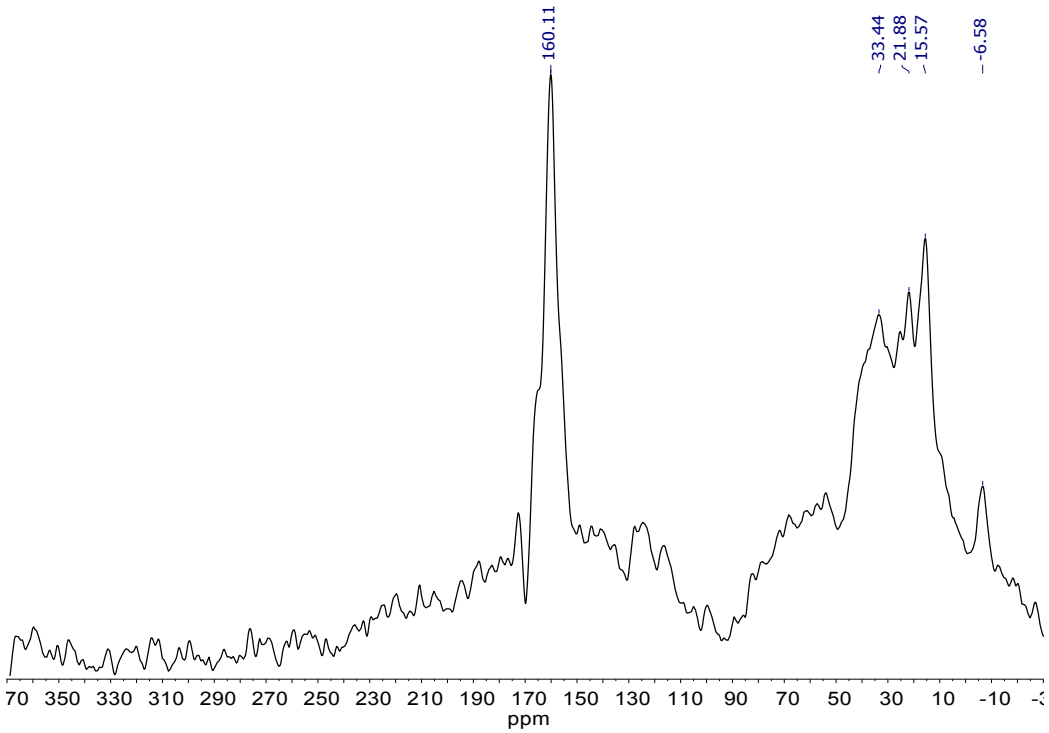

Figure S30. ^{13}C solid state NMR spectrum of Mg_3AlSO_4-W(NDipp)Me_3Cl.

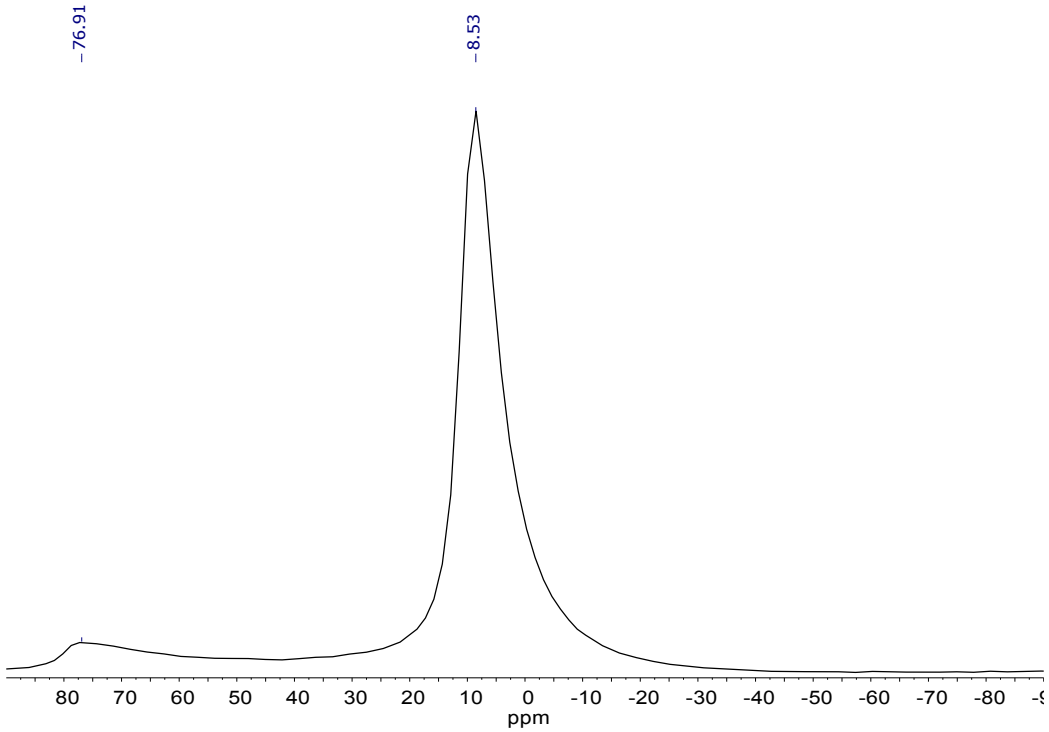

Figure S31. ^{27}Al solid state NMR spectrum of Mg_3AlSO_4-W(NDipp)Me_3Cl.

Infrared spectroscopy

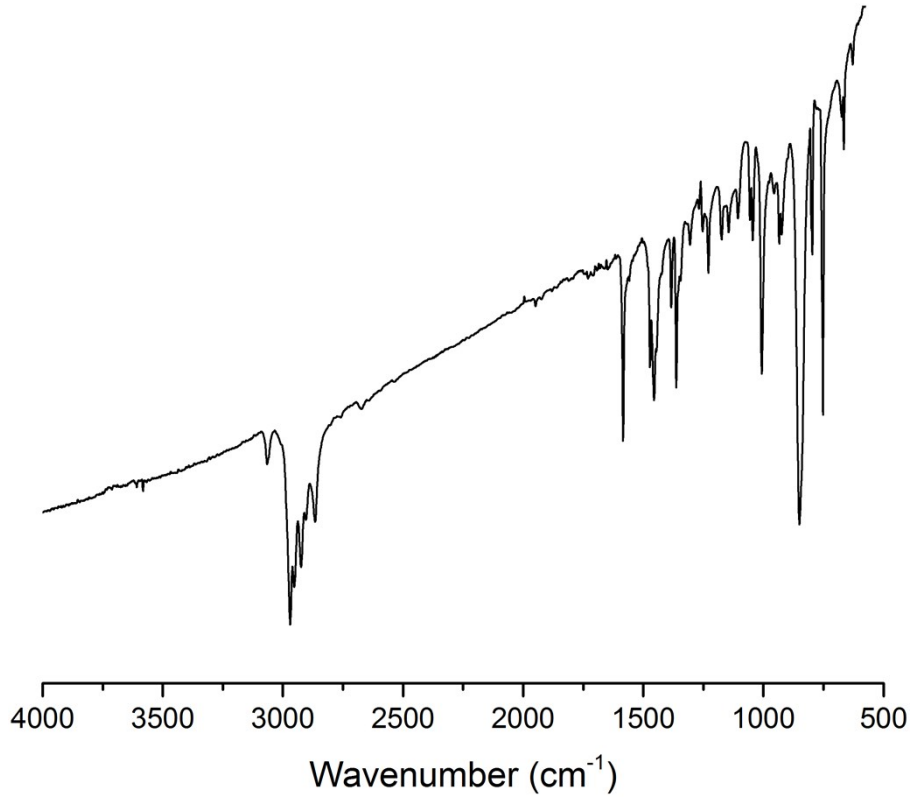

Figure S32. IR spectrum of $W(NDipp)Cl_4$.

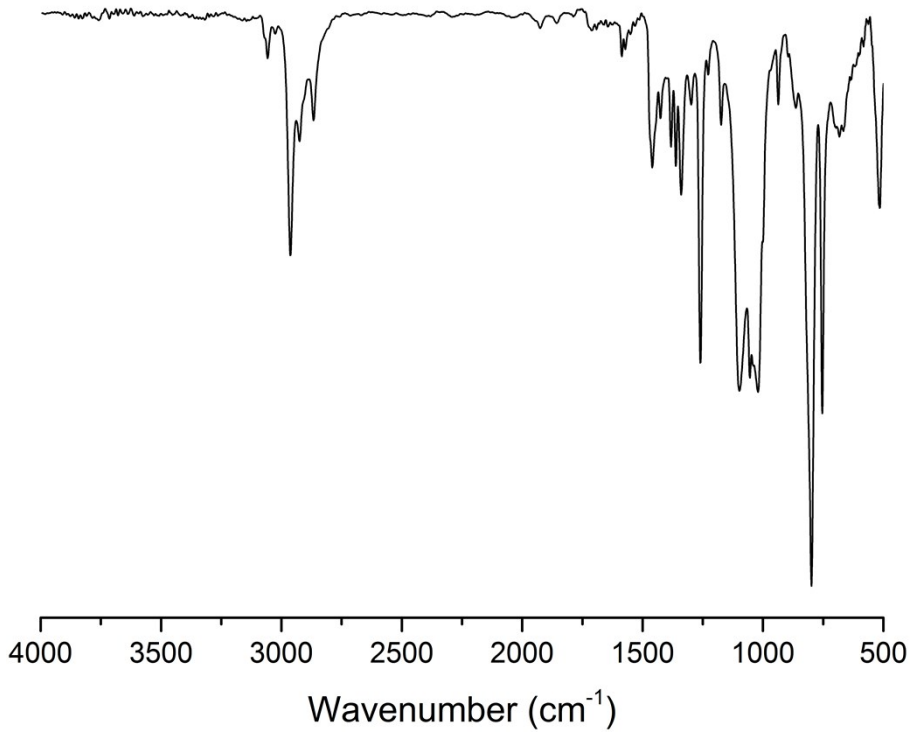

Figure S33. IR spectrum of $W(NDipp)Me_3Cl$.

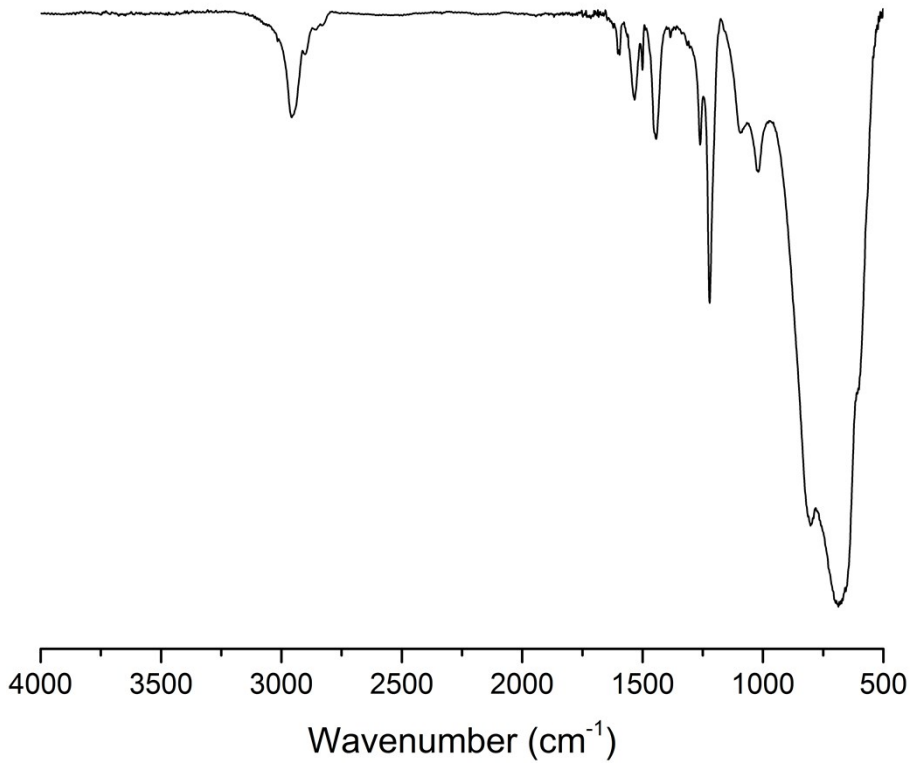

Figure S34. IR spectrum of W(NDipp)Cl_4(THF) supported on polymethylaluminoxane.

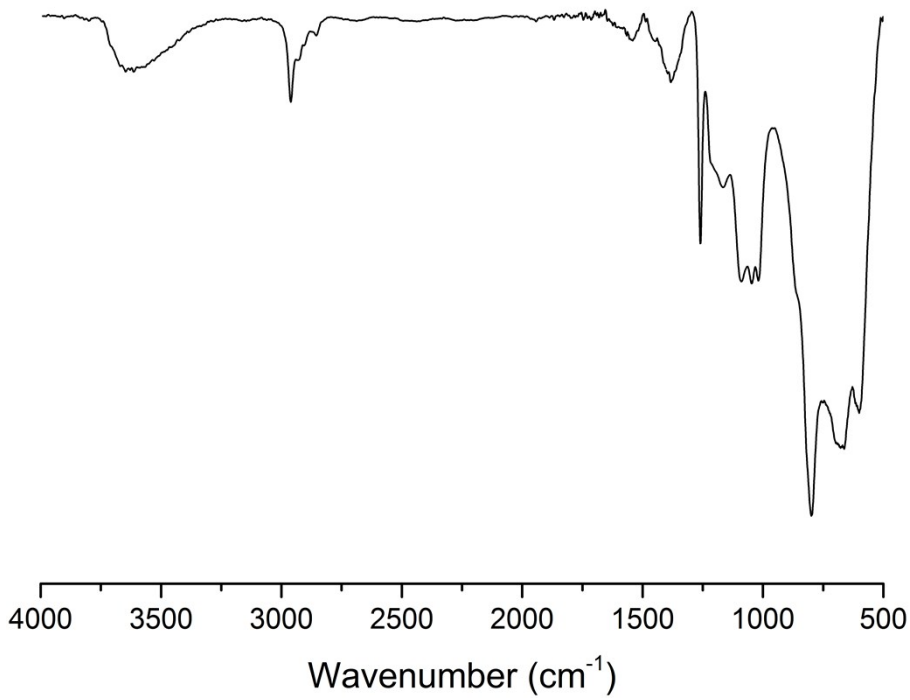

Figure S35. IR spectrum of W(NDipp)Cl_4(THF) supported on Mg_3AlSO_4-MAO.

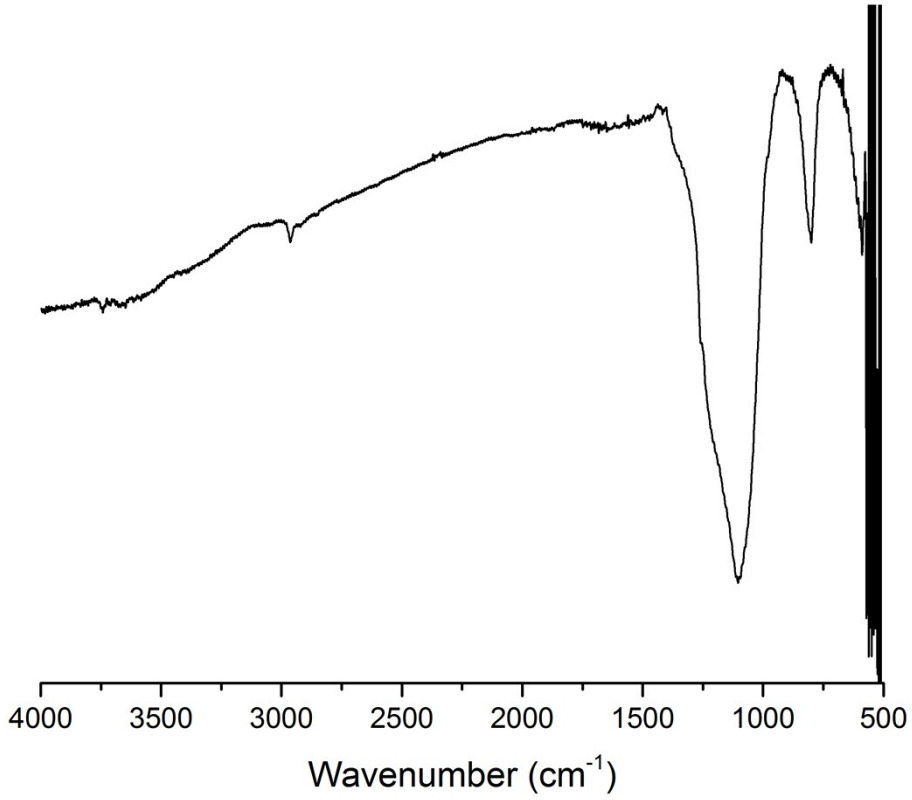

Figure S36. IR spectrum of silica.

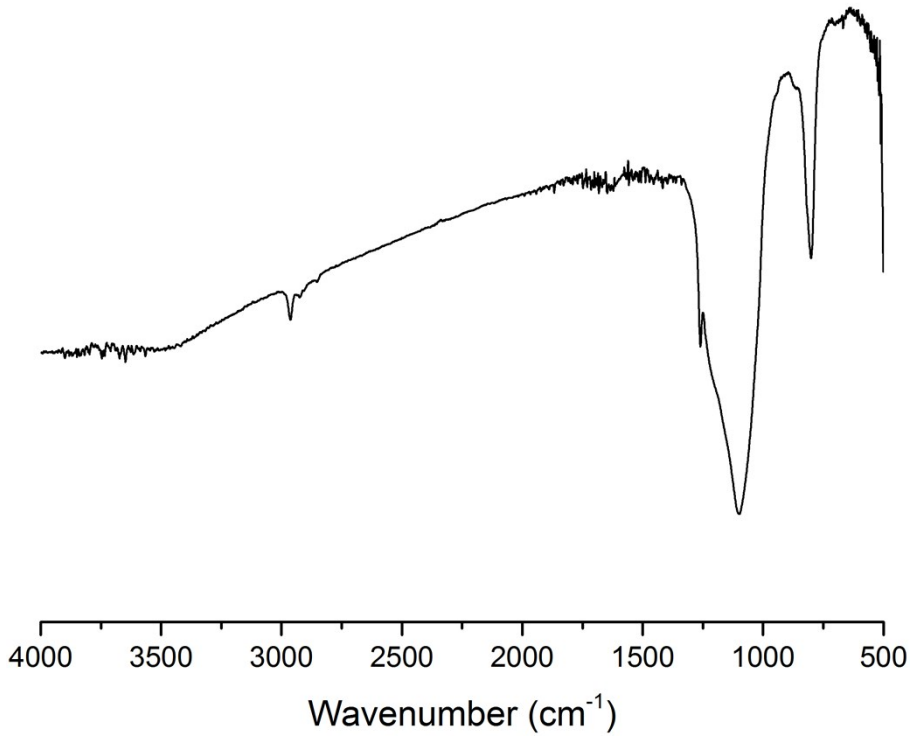

Figure S37. IR spectrum of W(NDipp)Cl_4(THF) supported on silica.

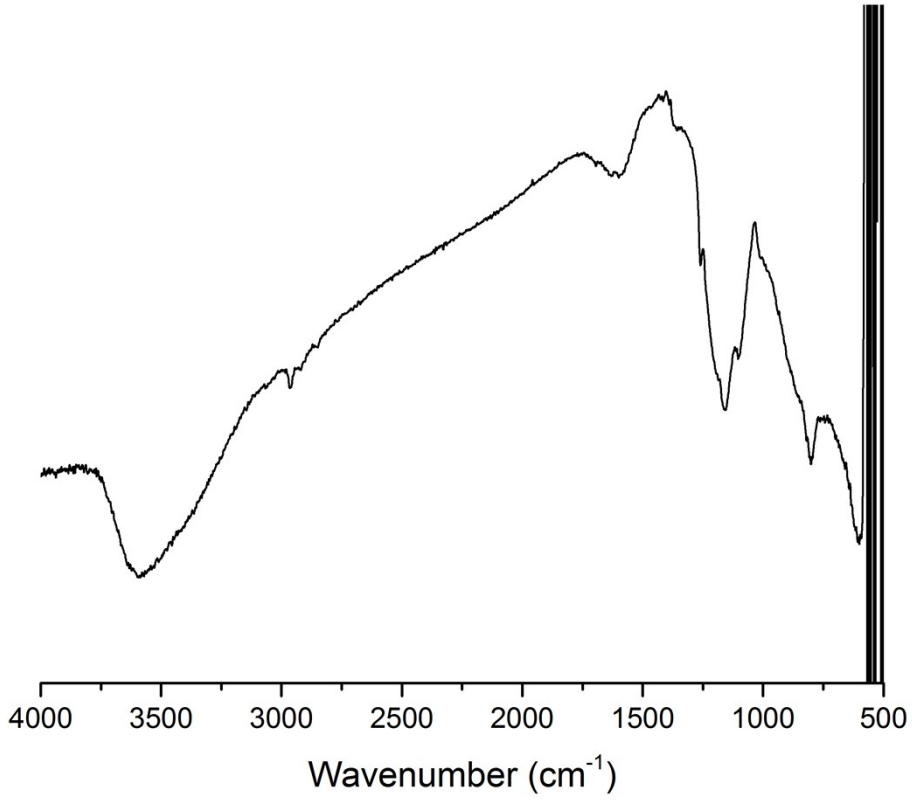

Figure S38. IR spectrum of Mg_3AlSO_4-LDH.

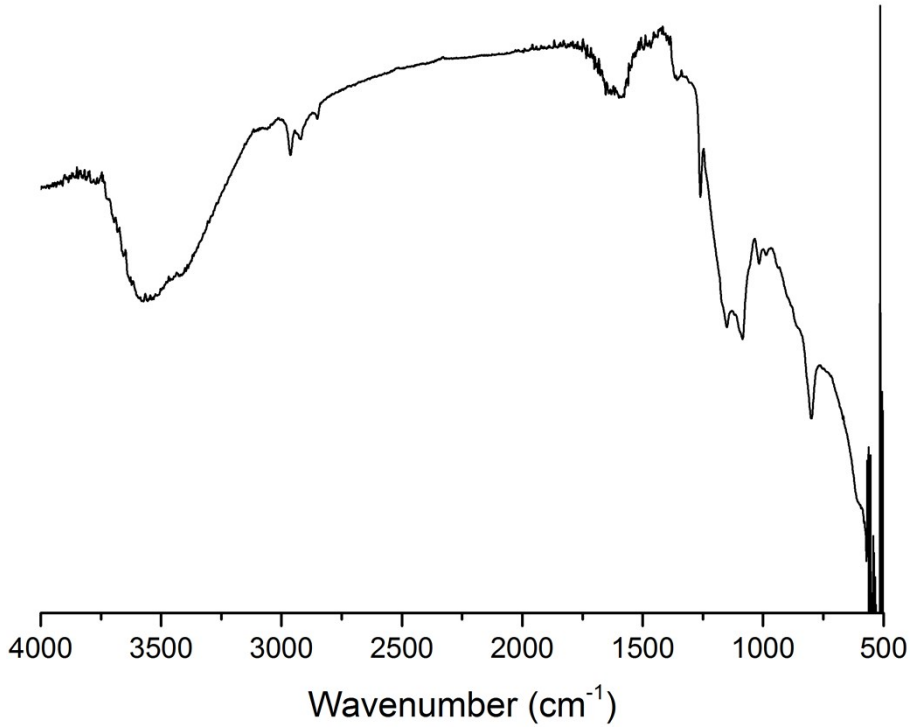

Figure S39. IR spectrum of W(NDipp)Cl_4(THF) supported on Mg_3AlSO_4-LDH.

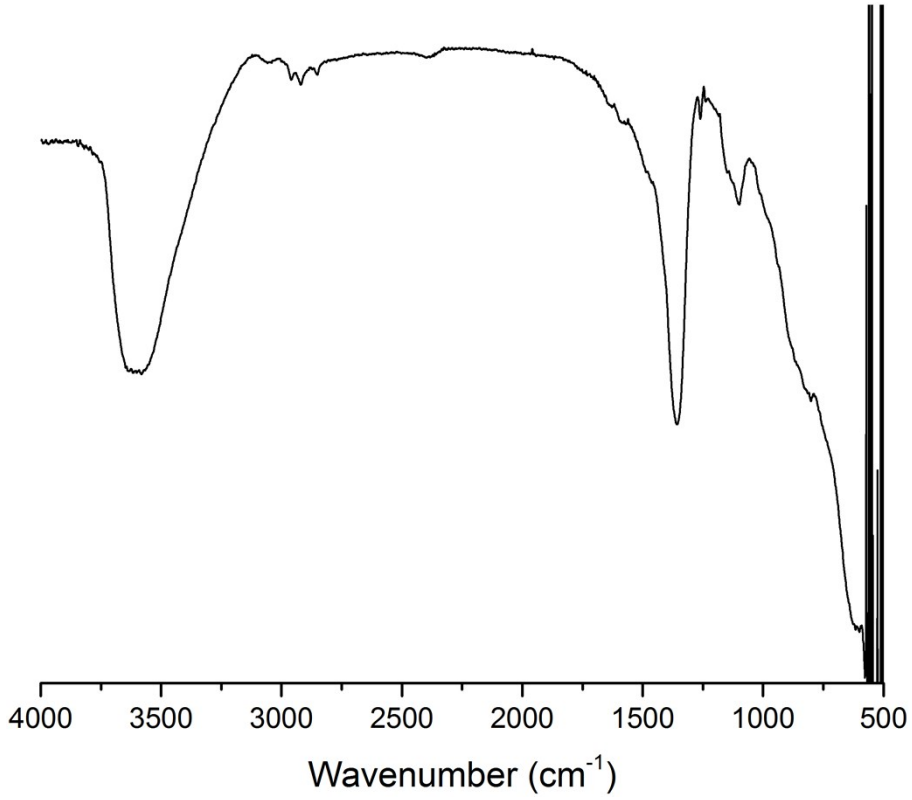

Figure S40. IR spectrum of Mg_3AlNO_3-LDH.

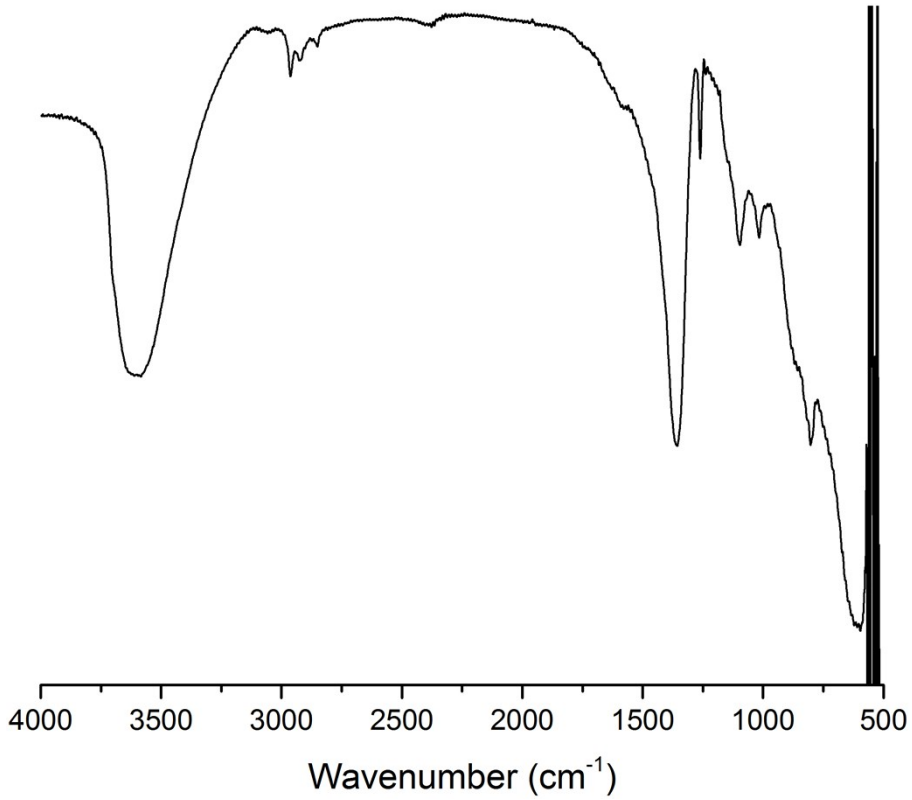

Figure S41. IR spectrum of W(NDipp)Cl_4(THF) supported on Mg_3AlNO_3-LDH.

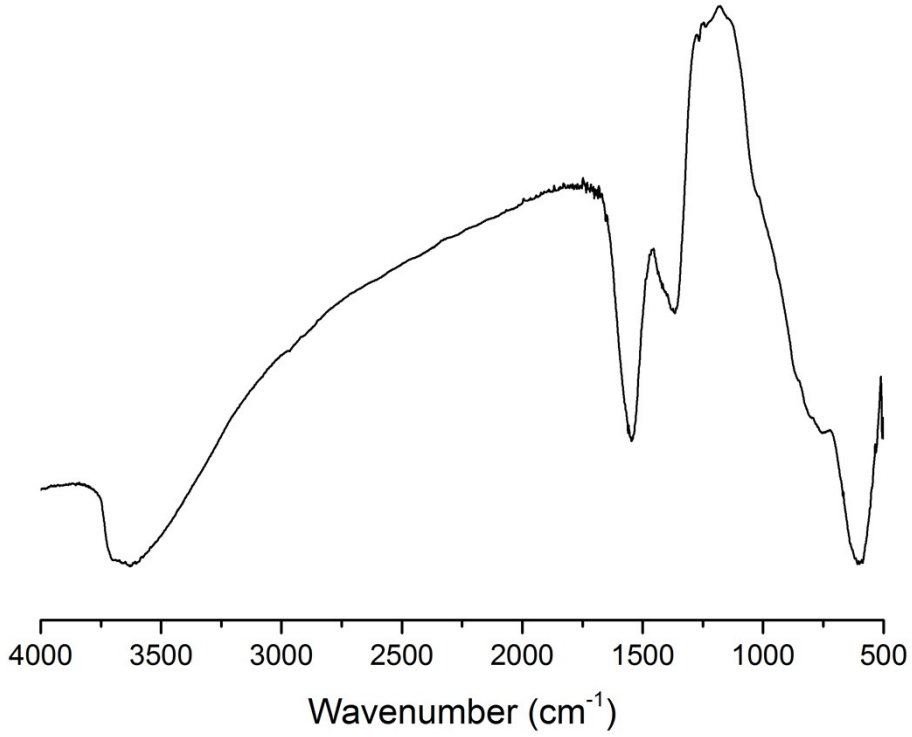

Figure S42. IR spectrum of Mg_3AlCO_3-LDH.

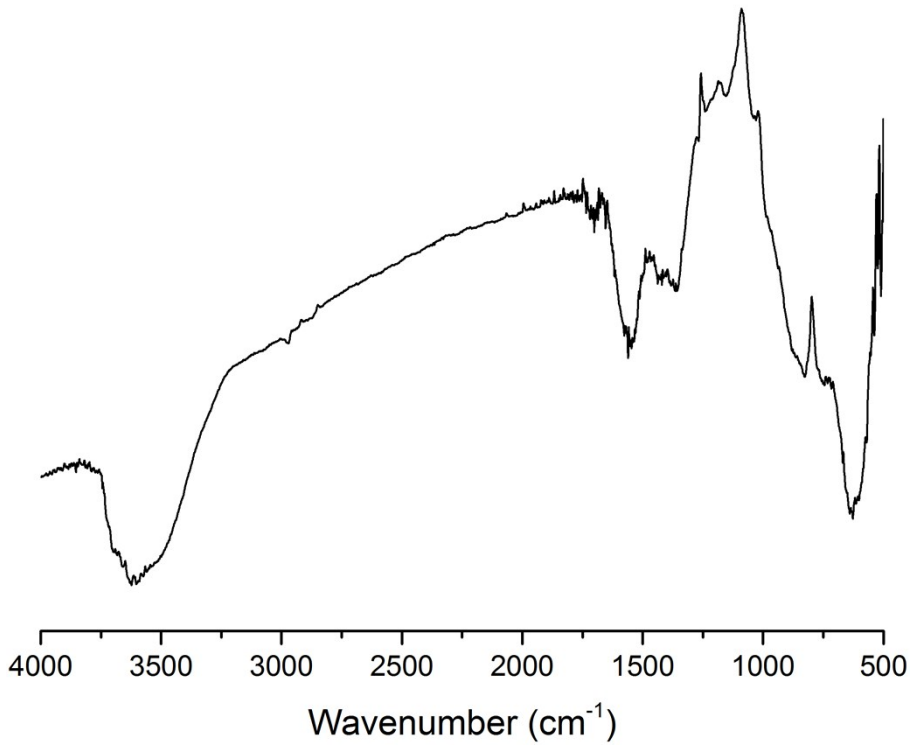

Figure S43. IR spectrum of $W(NDipp)Cl_4(THF)$ supported on Mg_3AlCO_3-LDH.

Solution ^{1}H NMR spectroscopy

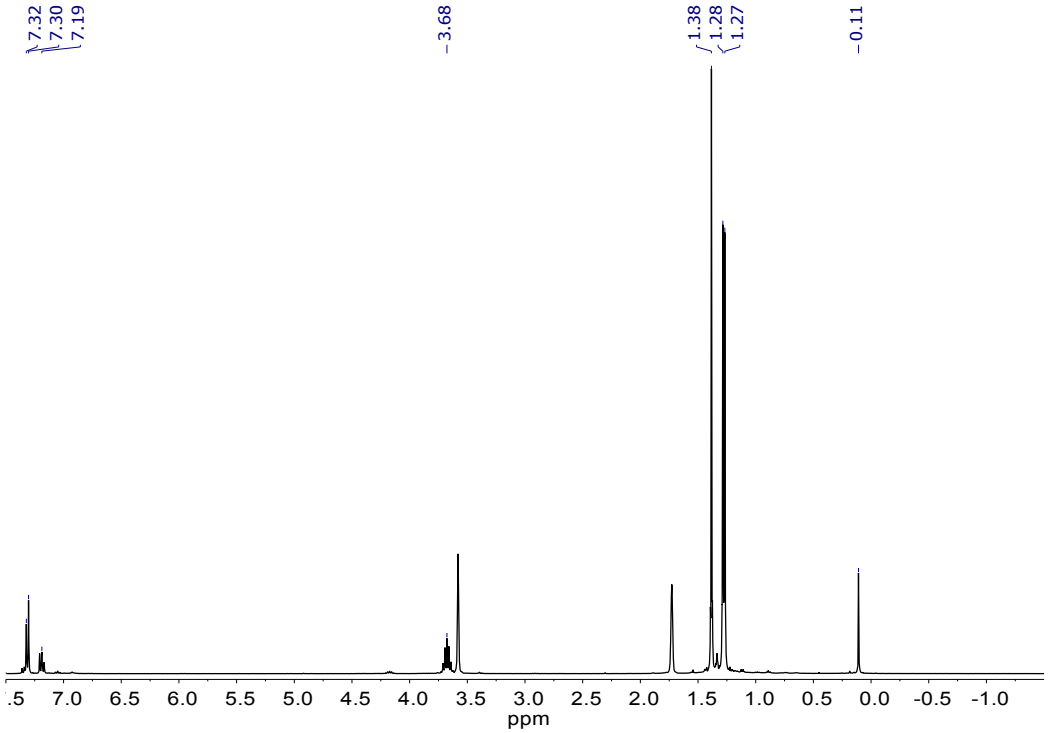

Figure S44. ^{1}H NMR spectrum of W(NDipp)Me_3Cl in C_4D_8O.

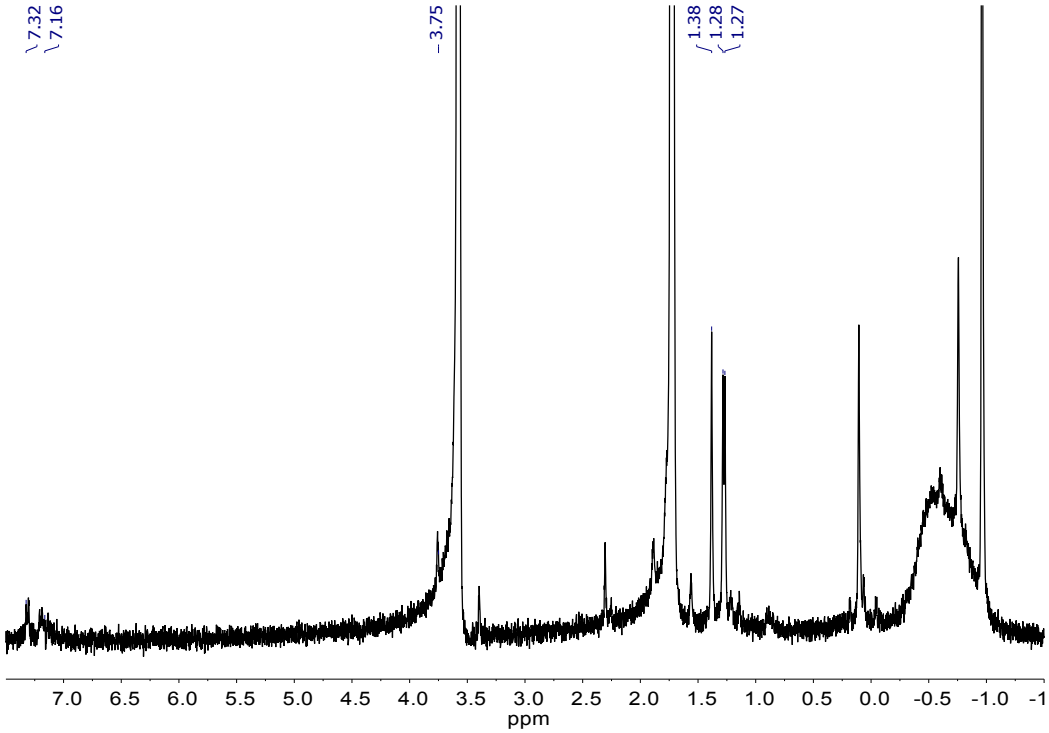

Figure S45. ^{1}H NMR spectrum in C_4D_8O of polymethylaluminoxane supported W(NDipp)Cl_4(THF) indicating leaching of the complex W(NDipp)Me_3Cl which is formed *in situ* on the surface.

6. Hetereogeneous oligomerisation studies

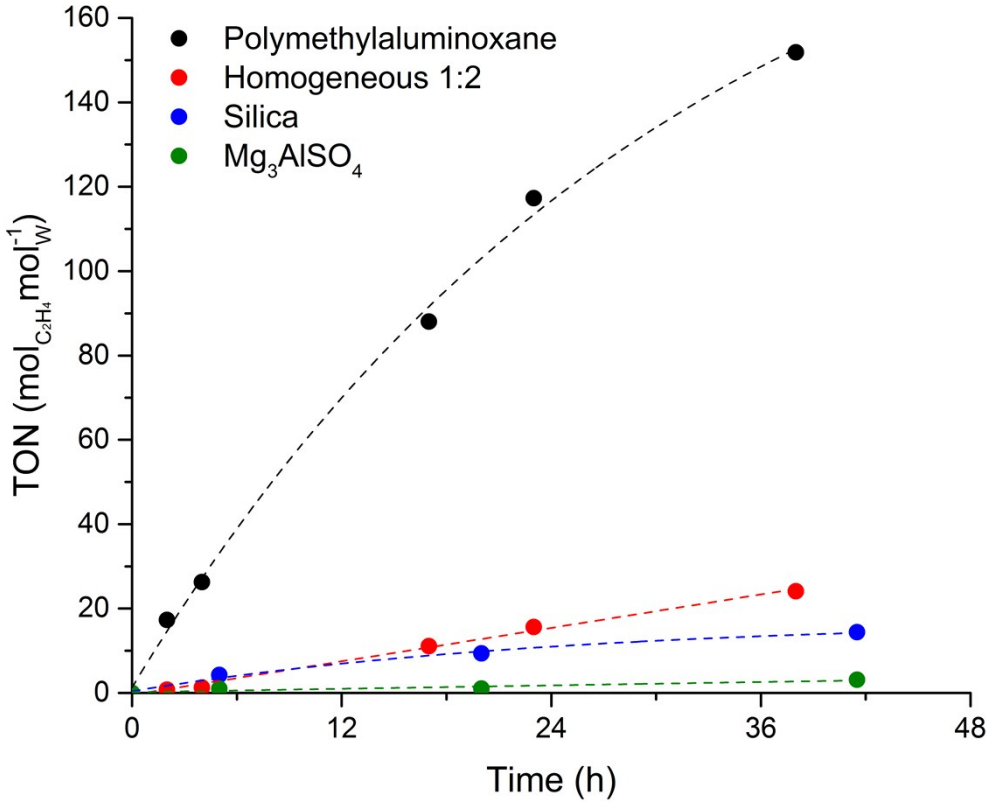

Figure S46. Comparison of the turnover numbers (TONs) of polymethylaluminoxane, silica and Mg_3AlSO_4 supported $W(NDipp)Cl_4(THF)$ with the homogeneous W:MAO = 1:2 reaction with 1 bar ethylene at 100 °C.

Table S14. Turnover numbers (TONs) for polymethylaluminoxane, silica and $MgAlSO_4$ supported $W(NDipp)Cl_4(THF)$.

Time/h	Polymethylaluminoxane TON/$mol_{C_2H_4}mol_W^{-1}h^{-1}$	Silica TON/$mol_{C_2H_4}mol_W^{-1}h^{-1}$	Mg_3AlSO_4 TON/$mol_{C_2H_4}mol_W^{-1}h^{-1}$
2	17.31		
4	26.25		
5		4.24	1.01
17	88.03		
20		9.39	1.06
23	117.31		
38	151.83		
41.5		14.39	3.13
55.5		18.68	5.15

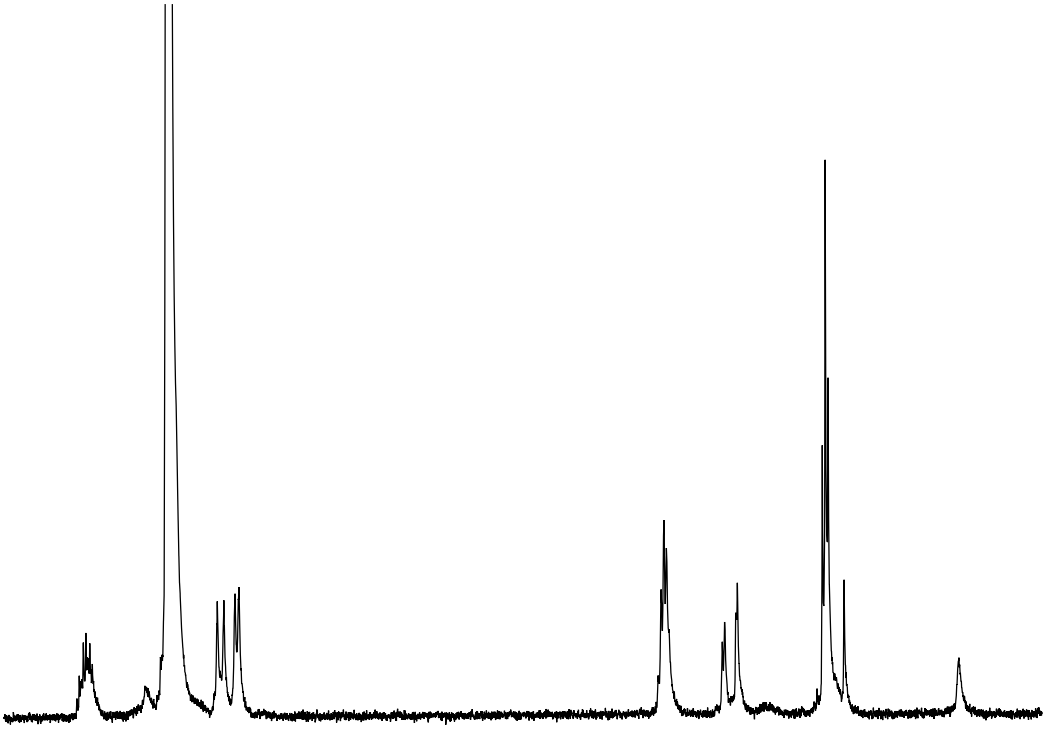

Figure S47. Gas phase reaction of polymethylaluminoxane supported W(NDipp)Cl_4(THF) showing formation of 1-butene at 100 °C and 1 bar ethylene in a Young's tap NMR tube.

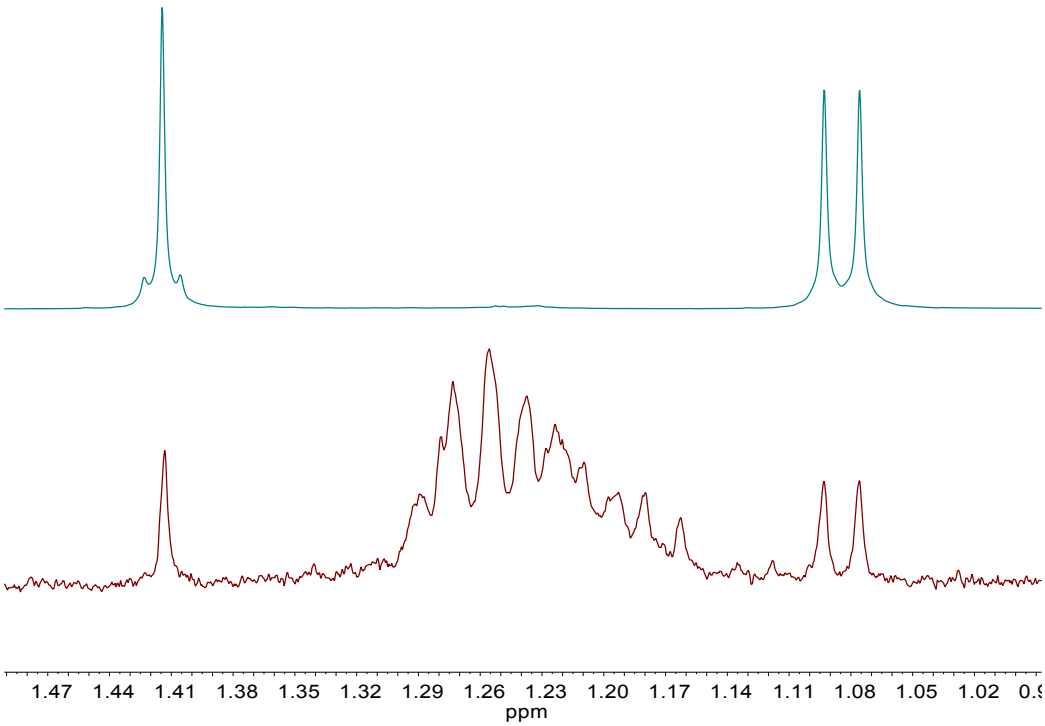

Figure S48. Top: Resonances corresponding to Me (1.41 ppm) and ^{i}Pr (1.08 ppm) of W(NDipp)Me_3Cl in C_6D_6. Bottom: Leached complex from W(NDipp)Me_3Cl supported on polymethylaluminoxane.

Oligomerisation reaction of W(NDipp)Me_3Cl supported on polymethylaluminoxane resulted in complex leaching into solution (Figure S48). The resulting inhomogeneous mixture was active for the dimerisation of ethylene, although isomerisation to 2-butenes and polymer formation were also observed. To test the stability of the polymethylaluminoxane species both W(NDipp)Cl_4(L) and W(NDipp)Me_3Cl supported catalysts were

heated to 100 °C in C_6D_6 containing an internal standard of pyridine. Leaching of the complex was only observed for the W(NDipp)Me_3Cl supported catalyst.

W(NDipp)$Me_3Cl(AlCl_3)$ To test the interaction between aluminium chloride and the tungsten methyl complex thought to form *in situ* on the surface which may explain the increased stability, W(NDipp)Me_3Cl (10 mg, 0.02 mmol) was contacted with anhydrous $AlCl_3$ (3 mg, 0.02 mmol) in C_6D_6. A downfield shift in the WCH_3 resonances was observed indicating increased positive charge on tungsten and hence Lewis adduct formation (Figure S49). The ^{27}Al NMR spectrum exhibited a resonance at 108 ppm indicative of a four coordinate aluminium species (Figure S50).

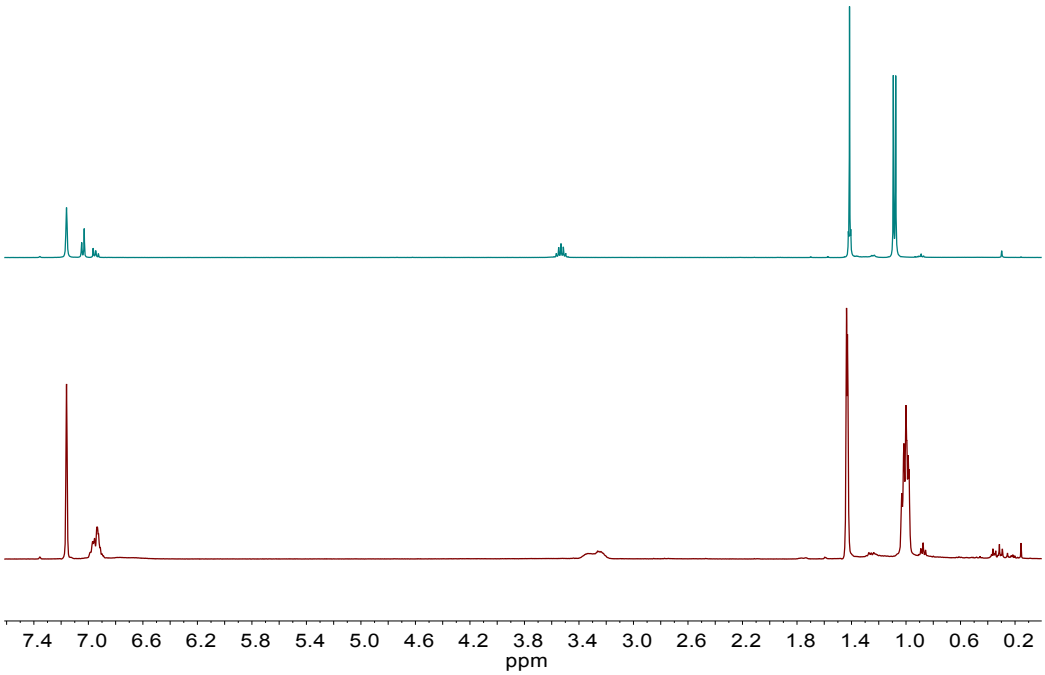

Figure S49. Top: W(NDipp)Me_3Cl in C_6D_6. Bottom: W(NDipp)Me_3Cl + $AlCl_3$ in C_6D_6.

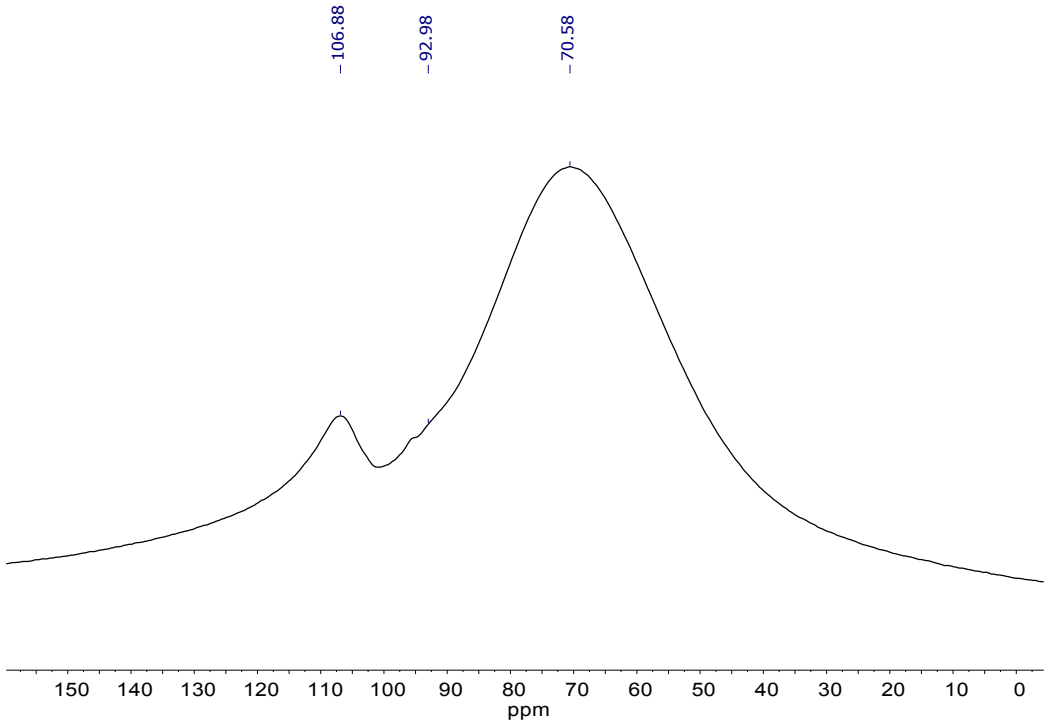

Figure S50. ^{27}Al NMR spectrum of W(NDipp)Me_3Cl +$AlCl_3$ in C_6D_6.

7. References

1. R. R. Schrock, R. T. DePue, J. Feldman, K. B. Yap, D. C. Yang, W. M. Davis, L. Park, M. DiMare, M. Schofield, J. Anhaus, E. Walborsky, E. Evitt, C. Krüger, and P. Betz, *Organometallics*, 1990, **9**, 2262–2275.
2. C. Chen, M. Yang, Q. Wang, J.-C. Buffet, and D. O'Hare, *J. Mater. Chem. A*, 2014, **2**, 15102–15110.
3. M. Yang, O. McDermott, J.-C. Buffet, and D. O'Hare, *RSC Adv.*, 2014, **4**, 51676–51682.
4. C. Chen, A. Wangriya, J.-C. Buffet, and D. O'Hare, *Dalt. Trans.*, 2015, **44**, 16392–16398.
5. E. Kaji and E. Yoshioka, 2010, WO2010055652.
6. CrysAlisPro, Oxford Diffraction/Agilent Technologies UK LTD, Yarnton, England.
7. Z. Otwinowski and W. Minor, in *Macromolecular Crystallography Part A*, ed. J. B. T.-M. in E. Charles W. Carter, Academic Press, 1997, vol. Volume 276, pp. 307–326.
8. R. H. Blessing, *Acta Crystallogr. Sect. A Fundam. Crystallogr.*, 1995, **51**, 33–38.
9. L. Palatinus and G. Chapuis, *J. Appl. Crystallogr.*, 2007, **40**, 786–790.
10. R. I. Cooper, A. L. Thompson, and D. J. Watkin, *J. Appl. Crystallogr.*, 2010, **43**, 1100–1107.
11. P. W. Betteridge, J. R. Carruthers, R. I. Cooper, K. Prout, and D. J. Watkin, *J. Appl. Crystallogr.*, 2003, **36**, 1487–1487.
12. L. J. Farrugia, *J. Appl. Crystallogr.*, 1999, **32**, 837–838.
13. L. J. Farrugia, *J. Appl. Crystallogr.*, 2012, **45**, 849–854.
14. A.L. Spek, *PLATON, a Multipurp. Crystallogr. tool, Utrecht, Netherlands*, 1998.
15. A. L. Spek, *J. Appl. Crystallogr.*, 2003, **36**, 7–13.
16. F. Neese, Orca - an ab initio, DFT and Semiempirical Electronic Structure Package, Version 2.8, Revision 2360,Institut für Physikalische und Theoretische Chemie, Universität Bonn, Bonn (Germany)).
17. A. D. Becke, *J. Chem. Phys.*, 1986, **84**, 4524.
18. J. P. Perdew and W. Yue, *Phys. Rev. B*, 1986, **33**, 8800–8802.
19. J. P. Perdew, *Phys. Rev. B*, 1986, **33**, 8822–8824.
20. E. van Lenthe, E. J. Baerends, and J. G. Snijders, *J. Chem. Phys.*, 1993, **99**, 4597.
21. E. van Lenthe, E. J. Baerends, and J. G. Snijders, *J. Chem. Phys.*, 1994, **101**, 9783.
22. E. van Lenthe, J. G. Snijders, and E. J. Baerends, *J. Chem. Phys.*, 1996, **105**, 6505.
23. D. A. Pantazis, X.-Y. Chen, C. R. Landis, and F. Neese, *J. Chem. Theory Comput.*, 2008, **4**, 908–919.
24. D. A. Pantazis and F. Neese, *J. Chem. Theory Comput.*, 2009, **5**, 2229–2238.
25. A. Schäfer, C. Huber, and R. Ahlrichs, *J. Chem. Phys.*, 1994, **100**, 5829.
26. F. Weigend and R. Ahlrichs, *Phys. Chem. Chem. Phys.*, 2005, **7**, 3297.
27. F. Weigend, *Phys. Chem. Chem. Phys.*, 2006, **8**, 1057.
28. K. Eichkorn, F. Weigend, O. Treutler, and R. Ahlrichs, *Theor. Chem. Accounts Theory, Comput. Model. (Theoretica Chim. Acta)*, 1997, **97**, 119–124.
29. K. Eichkorn, O. Treutler, H. Öhm, M. Häser, and R. Ahlrichs, *Chem. Phys. Lett.*, 1995, **240**, 283–290.
30. K. Eichkorn, O. Treutler, H. Öhm, M. Häser, and R. Ahlrichs, *Chem. Phys. Lett.*, 1995, **242**, 652–660.
31. E. F. Pettersen, T. D. Goddard, C. C. Huang, G. S. Couch, D. M. Greenblatt, E. C. Meng, and T. E. Ferrin, *J. Comput. Chem.*, 2004, **25**, 1605–1612.